AGU PUBLICATIONS

Tectonics

RESEARCH ARTICLE
10.1002/2013TC003357

Key Points:
- Provenance terranes of Permian arc basin sediments were identified
- Tectonic activity related to final ocean closure ceased by early Triassic
- A complex Permian arc geometry is recognized

Supporting Information:
- Readme
- Table S1
- Table S2
- Table S3
- Table S4
- Table S5

Correspondence to:
G. Zhao,
gzhao@hkucc.hku.hk

Citation:
Eizenhöfer, P. R., G. Zhao, J. Zhang, and M. Sun (2014), Final closure of the Paleo-Asian Ocean along the Solonker Suture Zone: Constraints from geochronological and geochemical data of Permian volcanic and sedimentary rocks, *Tectonics*, *33*, 441-463, doi:10.1002/2013TC003357.

Received 20 APR 2013
Accepted 1 MAR 2014
Accepted article online 13 MAR 2014
Published online 11 APR 2014

Final closure of the Paleo-Asian Ocean along the Solonker Suture Zone: Constraints from geochronological and geochemical data of Permian volcanic and sedimentary rocks

Paul R. Eizenhöfer[1], Guochun Zhao[1], Jian Zhang[1], and Min Sun[1]

[1]Department of Earth Sciences, University of Hong Kong, Pokfulam Road, Hong Kong, China

Abstract There is a broad consensus that the Solonker Suture Zone marks the final closure of the Paleo-Asian Ocean, which led to the formation of the eastern segment of the Central Asian Orogenic Belt. However, when and how the final closure occurred still remains controversial. To address this issue, provenance analysis of Permian sedimentary rocks of arc basins along the Xar Moron River was carried out. Geochemical analysis revealed a close relationship between the sedimentary and volcanic rock suite in the study region suggesting short transport distances and a complex convergent arc setting. Detrital zircon U-Pb analysis identified two major age provenances: (1) the Precambrian basement of the North China Craton (~2497 Ma and ~1844 Ma) and (2) the Paleozoic Southern Accretionary Orogen along the northern margin of North China (~436 Ma and ~269 Ma). The present locations of identified age provenances indicate southward subduction beneath the northern margin of North China. A comparison of the youngest age population in the sedimentary rocks with U-Pb ages obtained for subduction-related volcanic rocks implies that the Solonker Suture Zone formed from the Late Permian to Early Triassic. The results of our study advocate a complex Permian arc system which was probably similar to present-day Southeast Asia.

1. Introduction

The Central Asian Orogenic Belt (CAOB), between the East European Platform, the Siberian Craton, and the combined Tarim and North China Cratons (Figure 1), is one of the largest Phanerozoic orogenic systems on Earth [*Cawood et al.*, 2009]. Despite numerous investigations, it is perhaps the least understood tectonic belt on the Eurasian continent [*Şengör et al.*, 1993; *Windley et al.*, 2007; *Wilhem et al.*, 2012; *Kröner et al.*, 2014, and references therein]. Its formation covers the entire variety of convergent plate tectonics: (1) accretion of accretionary wedges, island arcs, terranes or microcontinents, and oceanic seamounts, and (2) continental collision, subduction, subduction roll-back, and back-arc spreading. Based on distinct geochemical differences, the CAOB has been termed an "internal" orogen in contrast to the circum-Pacific "external" orogens. Whereas "external" orogens are formed at the boundary of large mantle convection cells, "internal" orogens form within a single long-lived mantle convection supercell [*Collins et al.*, 2011].

The relationship between major tectonic blocks involved in the formation of the CAOB is still controversial. For example, the existence of blocks that rifted from the northern margins of Gondwana, or possibly from Siberia, in the Precambrian is still debated [e.g., *Wilhem et al.*, 2012; *Rojas-Agramonte et al.*, 2011]. The extent of volcanic arc chains situated in the open oceans between major tectonic units, such as the Paleo-Asian Ocean between the North China and Siberian Cratons, is unknown. Final disappearance of the Paleo-Asian Ocean terminated the formation of the CAOB, leading to collision between the combined Tarim and North China Cratons and the southern accretionary margin of the Siberian Craton in the Late Paleozoic and/or Early Mesozoic time. This ultimately formed the nearly east–west-trending Tian-Shan Suture located in Central Asia and the Solonker Suture Zone in East Asia [*Xiao et al.*, 2009].

Several tectonic models have been proposed to explain the formation and evolution of the CAOB. The classic, and repeatedly modified [e.g., *Yakubchuk*, 2008], single-arc model was initially proposed by *Şengör et al.* [1993]. It suggests that the main elements of the CAOB were derived from the successive roll-back, accretion, strike-slip faulting, and oroclinal bending of a single (or multiple) ocean spanning arc system, known as the

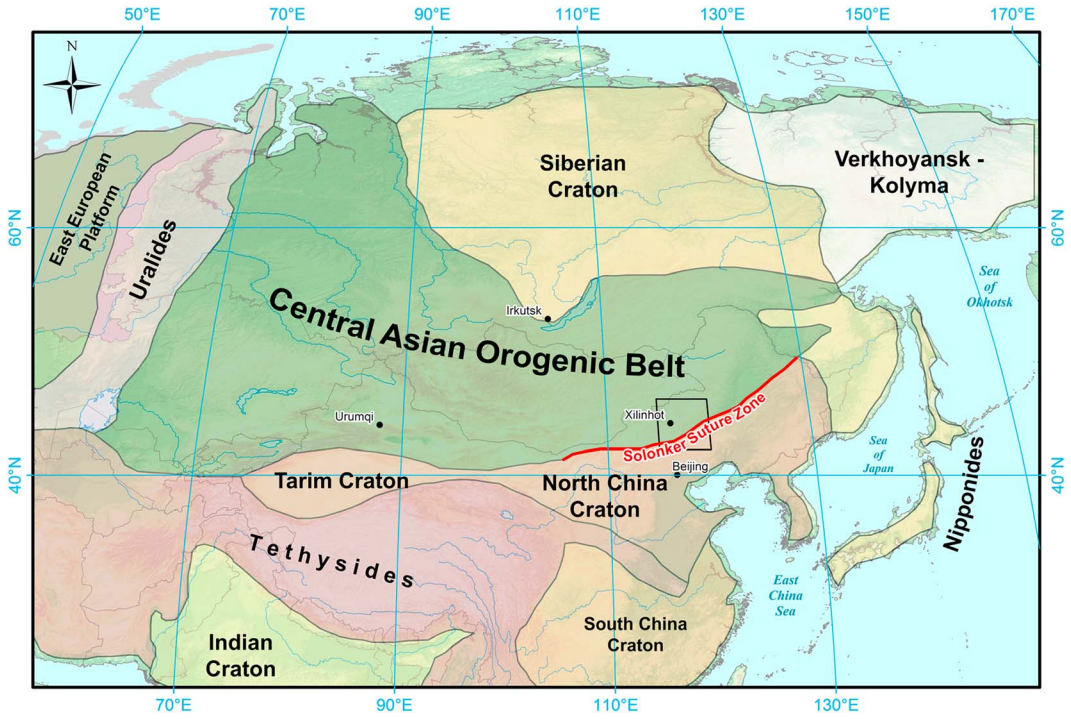

Figure 1. Tectonic subdivision of central and East Asia. A square outlines the study area across the Solonker Suture Zone (modified after *Şengör et al.* [1993]).

Kipchak-Tuva-Mongol arc. However, more recent paleomagnetic data, constraining the paleogeographic positions of the Siberian Craton and the East European Platform in Neoproterozoic time [*Smethurst et al.*, 1998; *Popov et al.*, 2005], and new structural data [*Lehmann et al.*, 2010] have challenged this model. Instead, an archipelago-type tectonic model has been brought forward [*Xiao et al.*, 2003, 2009, 2010; *Windley et al.*, 2007], which resembles modern-day Southeast Asia [e.g., *Hall*, 2009]. In this model, distinct volcanic arcs and terranes were accreted onto the active margins of the Siberian Craton and the East European Platform from the Early Paleozoic to the Late Permian/Early Mesozoic. *Lehmann et al.* [2010] modified the archipelago-type model by postulating initial east–west-directed shortening, followed by north–south-directed shortening based on extensive structural analyses. The extent to which accretion occurred along the northern margins of the Tarim and North China Cratons before the formation of the Solonker Suture Zone, however, remains a matter of debate [e.g., *Xiao et al.*, 2003; *Jian et al.*, 2008].

A large number of issues related to the paleogeographic geometry and origins of major tectonic units in the CAOB have not been satisfactorily resolved. A more detailed understanding is needed with respect to the development of volcanic arcs, the relative paleogeographic location of terranes before the final closure, and the interaction between respective tectonic elements within the Paleo-Asian Ocean. The current definition of major tectonic units in the eastern segment of the CAOB by different workers [e.g., *Xiao et al.*, 2003; *Jian et al.*, 2008, 2010] is confusing due to the inconsistent nomenclature of tectonic units and their locations. Figure 2 is an attempt to standardize the nomenclature of tectonic units in the region based on a combination of literature review [*Bureau of Geology and Mineral Resources of Inner Mongolia* (*BGMRIM*), 1991; *Xiao et al.*, 2003, 2009; *Jian et al.*, 2008, 2010] and the results of this study.

Detrital U-Pb zircon geochronology of Late Paleozoic sedimentary arc basins located in the Paleo-Asian Ocean is a potentially powerful tool with which to quantitatively evaluate issues of when and how the Paleo-Asian Ocean was closed to form the Solonker Suture Zone. It provides information on relationships between major tectonic blocks, such as their relative paleogeographic locations in time or contribution to sedimentary material [*Haughton et al.*, 1991]. Major tectonic units can be identified by comparing age distributions to well-defined "age-fingerprints" of likely provenance terrane candidates.

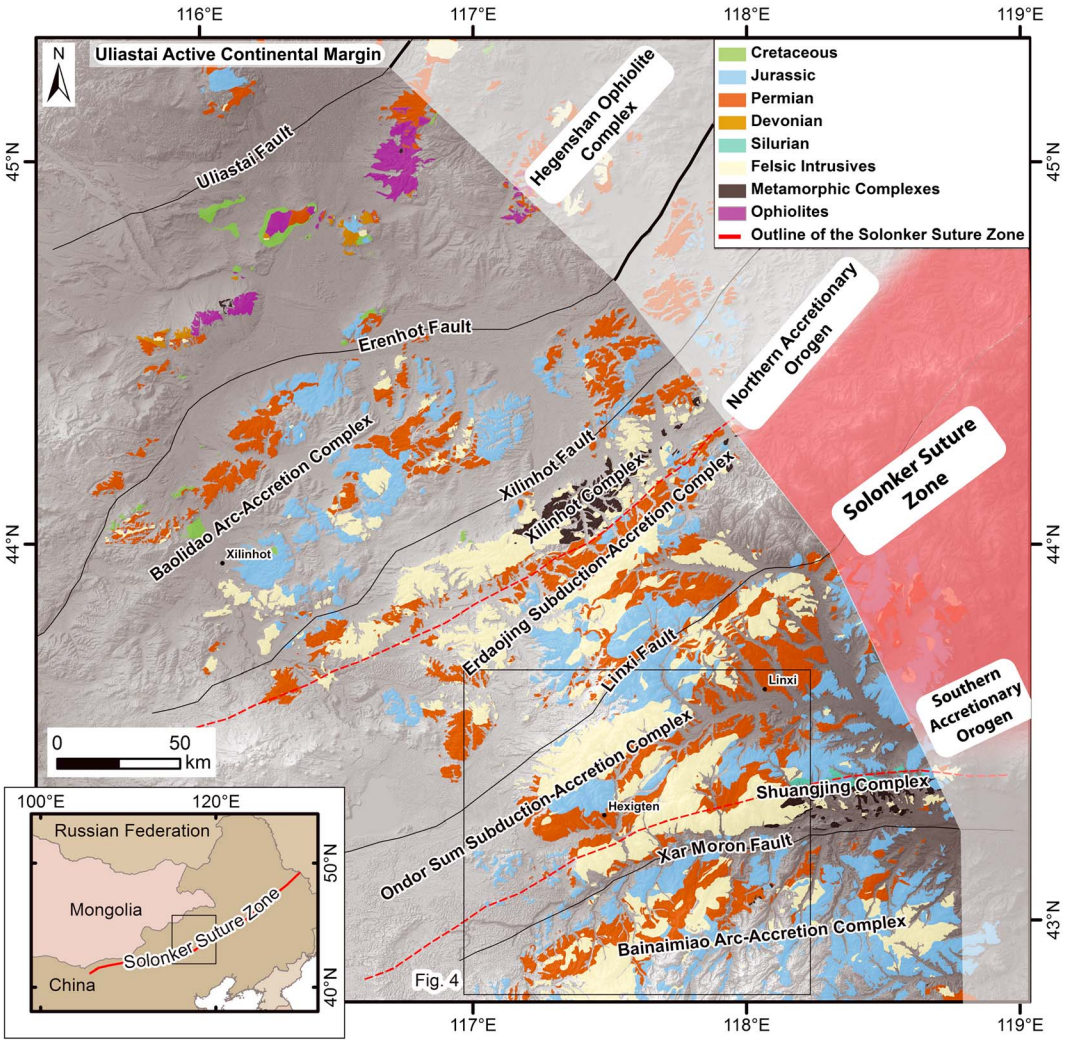

Figure 2. Tectonic subdivision of the Solonker Suture Zone in the Xilinhot area, based on new data presented in this study and literature review [*BGMRIM,* 1991; *Xiao et al.,* 2003, 2009; *Jian et al.,* 2008, 2010].

The Solonker Suture Zone has long been considered to mark the location of the final disappearance of the Paleo-Asian Ocean in the eastern segment of the CAOB. However, the time of final suturing and its exact location are still contended [e.g., *Li et al.*, 2013; *Xu et al.*, 2013]. More detailed investigations and an extensive regional geochronological analysis will further refine and update exact timing of major collisional, magmatic, and metamorphic events during the closure of the Paleo-Asian Ocean along this crucial collision zone.

This work evaluates the timing of the final closure of the Paleo-Asian Ocean and identifies major sedimentary provenance terranes along the Solonker Suture Zone. Integration of geochronological, geochemical, structural data, and field observations are used to provide an updated view of the tectonic evolution of the region in the Paleozoic until final suturing.

2. Regional Geology

2.1. Solonker Suture Zone

There has been much debate on whether the Solonker Suture Zone was formed by episodic [*Jian et al.*, 2008, 2010] or continuous [*Chen et al.*, 2000, 2009a; *Xiao et al.*, 2003] tectonic activity caused by subduction of oceanic lithosphere. The question of whether the final collision took place by southward subduction beneath the northern margin of North China or northward subduction beneath the southern accretionary margin of the Siberian Craton, as well as the actual subduction type (continental or oceanic) and its geometry (one sided,

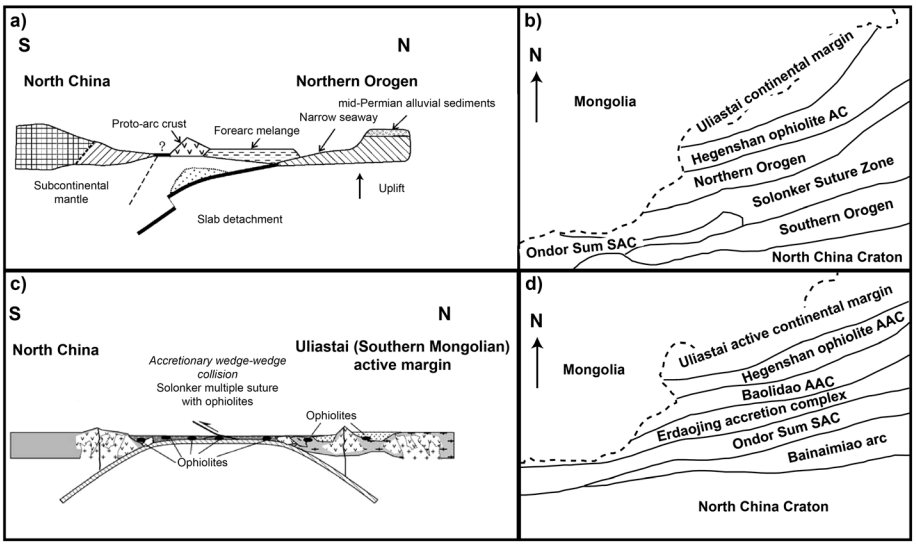

Figure 3. Formation of the Solonker Suture Zone during the Late Permian. (a) Single-sided subduction model according to *Jian et al.* [2008, 2010] with its (b) tectonic subdivision and (c) double-sided subduction model according to *Xiao et al.* [2003, 2009] with its (d) tectonic subdivision. AAC: arc-accretion complex; SAC: subduction-accretion complex; AC: accretion complex.

double sided, multiple), remains unresolved. Most researchers [e.g., *Wu et al.*, 2002, 2007; *Xiao et al.*, 2003; *de Jong et al.*, 2006; *Li*, 2006; *Shen et al.*, 2006; *S. H. Zhang et al.*, 2007, 2009; *X. H. Zhang et al.* 2009; *Jian et al.*, 2008, 2010; *Lin et al.*, 2008; *Chen et al.*, 2009a] locate the final closure of the Paleo-Asian Ocean along the banks of the Xar Moron River. *Wu et al.* [2002, 2007] traced it farther toward the far east, where it was offset by several major fault systems (the Yitong-Yilan Fault and the Dunhua-Mishan Fault), away from the Xar Moron River. However, some other authors [e.g., *Shao*, 1989; *Tang*, 1990; *Nozaka and Liu*, 2002] assume that the final collision took place further north near the Hegenshan Ophiolite Complex [*Miao et al.*, 2008] varying from end of the Devonian to the Middle Mesozoic, respectively, which are both temporally and spatially contrary to recent models.

According to the model proposed by *Li* [2006] and *Jian et al.* [2008, 2010], the Solonker Suture Zone is located along the northern bank of the Xar Moron River. Northward, it is bounded by the northeast trending Linxi Fault and southward by the northeast oriented Xar Moron Fault (Figures 3a and 3b). The Linxi Fault separates the Solonker Suture Zone from an accretionary belt named the Northern Orogen (Figure 3b) [*Jian et al.*, 2008], which comprises several accretionary and metamorphic complexes including the Xilinhot Complex along the Xilinhot Fault [*Shi et al.*, 2003; *Chen et al.*, 2009b]. Situated south of the Solonker Suture Zone defined by *Jian et al.* [2008] is the Southern Orogen (Figure 3b), which is considered to have successively developed along the northern margin of North China during Paleozoic. The orogen comprises subduction-accretion assemblages including the Ondor Sum Subduction-Accretion Complex [*Yan et al.*, 1989; *de Jong et al.*, 2006; *Chen et al.*, 2009a], whereas earlier outdated studies assumed the existence of an east–west trending "Wendur Miao–Xar Moron Ophiolite Belt" [see *Cao*, 1989]. *Jian et al.* [2008, 2010] argued that the North China and Siberian cratons were separated by the Paleo-Asian Ocean and microcontinents during the Cambrian. By the end of the Cambrian, the intraoceanic southward subduction led to arc volcanism and ophiolite formation, while northward subduction occurred beneath a microcontinent. Subsequently, concurrent ridge subduction beneath the volcanic arcs in the south and north caused high-grade metamorphism in the Ordovician and the Silurian. The end-Silurian collision of several microcontinents finally terminated subduction on both sides by forming the Southern and Northern Orogens, while they were still separated by the Paleo-Asian Ocean. During Early Permian time, tectonic activity continued with subduction, arc formation, and ridge-trench collision along the Southern Orogen. By then, the Southern Orogen was amalgamated with the northern margin of North China. Meanwhile, bimodal volcanism occurred in the Northern Orogen. The final closure of the Paleo-Asian Ocean in the Late Permian led to the formation of the Solonker Suture Zone (Figure 3a).

The model by *Xiao et al.* [2003, 2009], however, proposes a slightly different subdivision of tectonic units in the region (Figures 3c and 3d). In their model the Solonker Suture Zone is represented by the Erdaojing

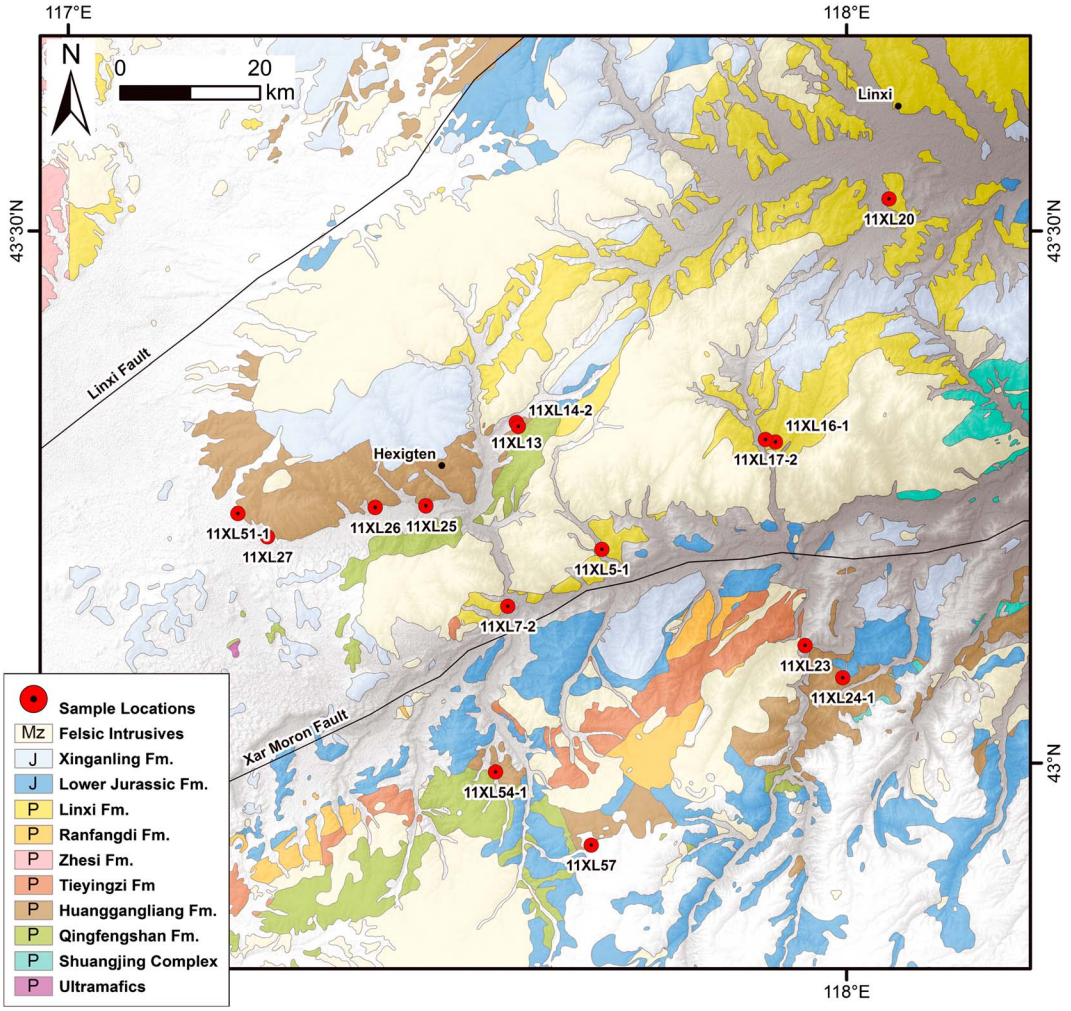

Figure 4. Geological map of the Xar Moron River region showing sample locations. Formations are described in text (after *BGMRIM* [1991]). Mz = Mesozoic; J = Jurassic; P = Permian.

Accretion complex. Thus, it is shifted to the north and is narrower. The Erdaojing Accretion Complex is juxtaposed toward north against the Baolidao Arc-Accretion Complex [*Chen et al.*, 2009a] and toward south with the Ondor Sum Subduction-Accretion Complex [*Yan et al.*, 1989; *de Jong et al.*, 2006]. Closure of the Paleo-Asian Ocean started with north-directed intraoceanic subduction, forming the Ulan Arc and the attached Ondor Sum Subduction-Accretion complex. In the Ordovician-Silurian, the Ulan Arc and the Ondor Sum Subduction-Accretion complex were accreted onto the northern margin of North China, while subduction took place southward beneath North China. Meanwhile, subduction had also been initiated along the southern margin of the Mongolian Arc Terranes, forming the Uliastai Active Continental Margin north of the Hegenshan Ophiolite Arc-Accretion Complex. The contemporary double-sided subduction beneath North China and the Mongolian Arc Terranes, as well as simultaneous intraoceanic subduction, led to the final closure of the Paleo-Asian Ocean in the Late Permian.

The above outlined two tectonic models [*Xiao et al.*, 2003, 2009; *Jian et al.*, 2008, 2010] (Figure 3) are different in their subduction geometries and definition of which tectonic units were involved during the closure of the Paleo-Asian Ocean. Notably, the suggested interactions between the tectonic units prior to the formation of the Solonker Suture Zone remain inconsistent, which is an issue to be addressed here. The study area extends across the Xar Moron River (Figure 4) and thus provides an ideal testing ground for both major tectonic models on the formation, and the location, of the Solonker Suture Zone.

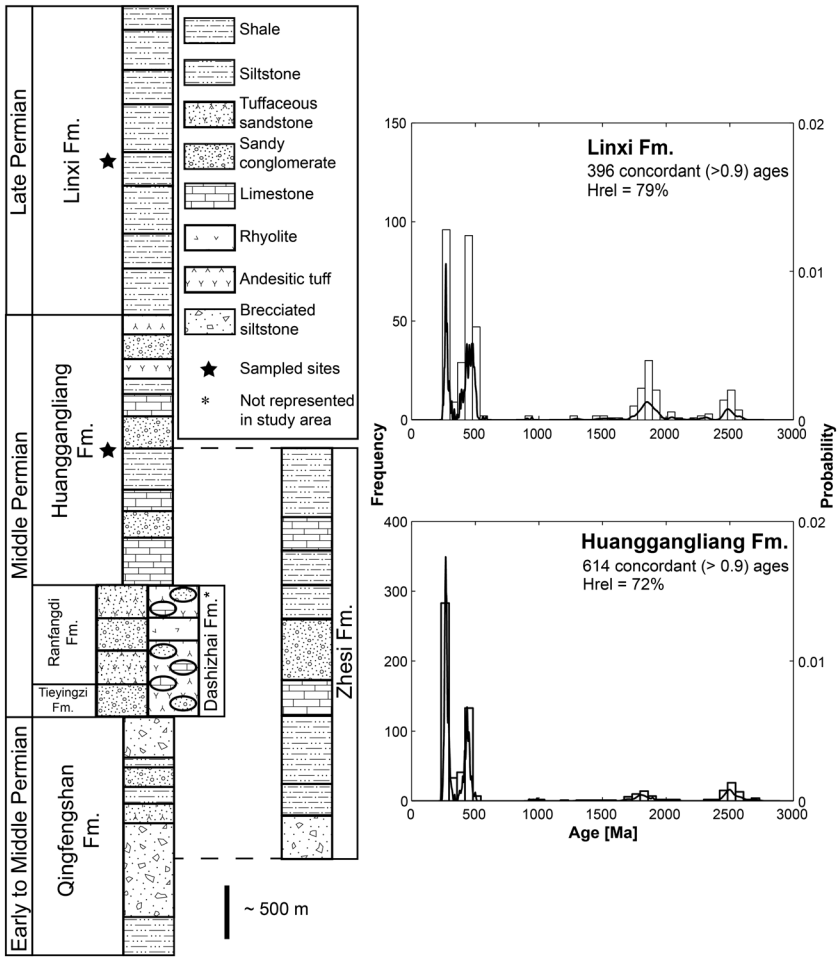

Figure 5. Permian stratigraphic column of the study area (after *Shen et al.* [2006]) and combined age distribution diagrams for the Huangganglian and Linxi formations. H_{rel} stands for the value of relative heterogeneity of an age probability distribution (see text for definition).

2.2. Geology Across the Xar Moron River

A Late Paleozoic stratigraphy of the region is relatively well established [*Li*, 2006; *Manankov et al.*, 2006; *Shen et al.*, 2006; *Shi*, 2006; *Shi et al.*, 2006]. The lithology across the Xar Moron River near Hexigten is dominated by broadly northeast trending Permian volcanoclastic turbiditic successions, represented dominantly by the Linxi and Huangganglian formations, and undeformed Mesozoic granitic intrusions (Figures 2 and 4–7). The volcanoclastic strata are subvertical without any signs of high-grade metamorphism. Open upright folds in the Huangganglian Formation (Figure 6) indicate a contractional strain regime. Both units are suggested to represent arc basin deposits, which is supported by their mineralogical immaturity and high volcanic detritus content (e.g., feldspars and volcanic lithic fragments). A single greenschist to amphibolite facies metamorphic unit, named the Shuangjing Complex (Figures 2 and 4) consisting of various schists [*Li et al.*, 2007; *Y. L. Li et al.*, 2011b], occurs along the northern bank of the Xar Moron River. Horizontally bedded Jurassic volcanic strata unconformably overlie the entire region (Figure 8a).

The Middle Permian Huangganglian Formation (marine strata) overlies the Middle Permian (Roadian to Wordian) Dashizhai Formation (also marine strata). The Dashizhai Formation per se does not occur in the study region. However, it is correlated with the volcanoclastic Tieyingzi and the overlying Ranfangdi Formation. The Huangganglian Formation is subdivided into an upper and a lower member, dominated by clastic and carbonate strata, respectively (Figure 5). These strata are unconformably overlain by the generally finer clastic Linxi Formation, which is considered to be terrestrial by some authors [e.g., *Shen et al.,* 2006]. However, a marine origin deems more likely since the study region marks the locus of the final closure of the

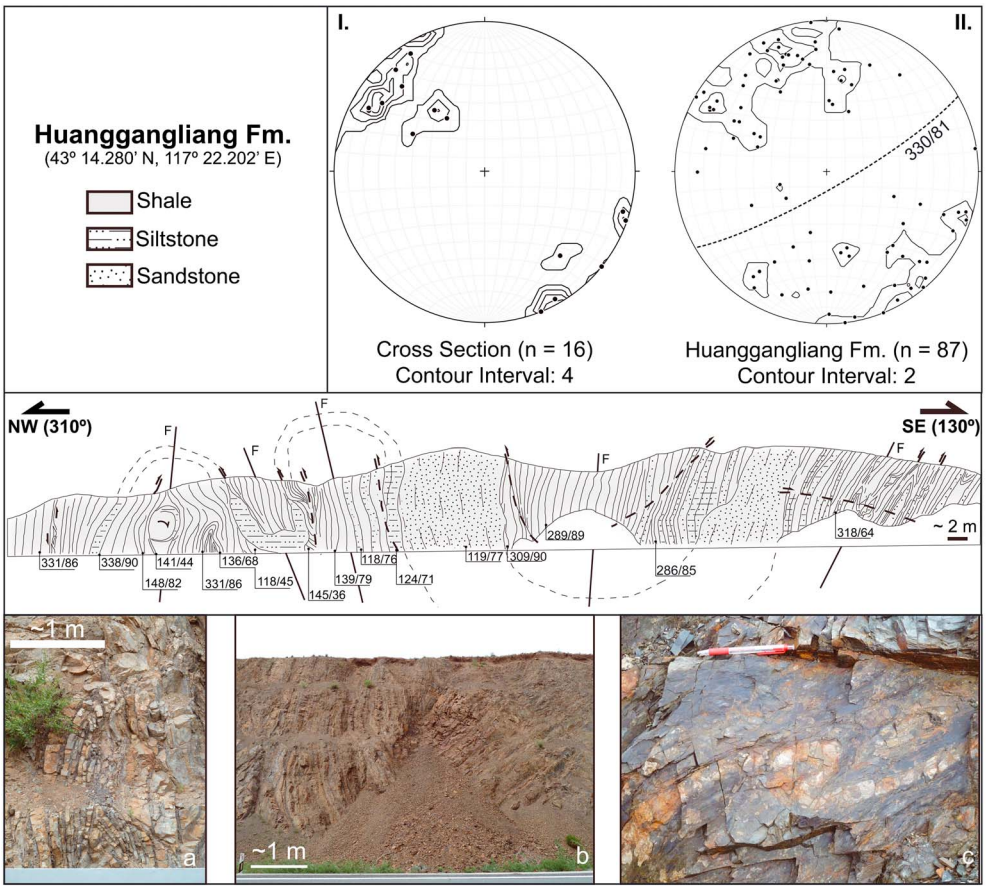

Figure 6. A cross section of turbiditic sequences with structural attitudes (dip azimuth/dip) in the Huangganglíang Formation. Photographs show (a) isoclinal fold, (b) open upright fold, and (c) shear fold observed in the formation. Stereonets show (I.) measurements of S_0 from the cross section and (II.) measurements of S_0 from the Huangganglíang Formation in the entire study area. The average of all measurements is projected as dashed great circle. F: fold plane.

Paleo-Asian Ocean. Our field observations confirm that the Linxi Formation consists of alternating sandstone, siltstone, and shale which occur on a regional scale, suggesting a turbiditic origin, although typical turbiditic patterns (e.g., cross-stratification, graded, or convolute bedding) are rare (Figure 7b).

Observed local faults are generally east-northeast striking, roughly parallel to the course of the Xar Moron River and the major regional Linxi and Xar Moron Faults. Cross sections along the Huangganglíang Formation (Figure 6) show open upright folding, thrust directions generally toward southeast or northwest, while shear folding, probably related to synsedimentary compression, can be observed as well. Thrusts are rare, if not absent, in the Linxi Formation (Figure 7).

The Permian sedimentary arc basins composed of the Huangganglíang and Linxi Formations are juxtaposed with arc-related rock assemblages, such as the Ondor Sum Subduction-Accretion Complex [*Yan et al.*, 1989; *de Jong et al.*, 2006] and the Erdaojing Subduction-Accretion Complex. However, the contact relationship between the sedimentary rocks and the tectonic units is not clear. Major tectonic units such as the North China Craton in the south and the Mongolian Arc Terranes further north are in relative regional vicinity. This central position provides an ideal laboratory to refine the timing of the final closure of the Paleo-Asian Ocean, location of the Solonker Suture Zone, and the interaction between the various major tectonic units.

3. Methodology

For this study we selected 15 samples collected in the Xar Moron River region. Eight were from the Middle Permian Huangganglíang Formation. Five samples were from the Upper Permian Linxi Formation. One

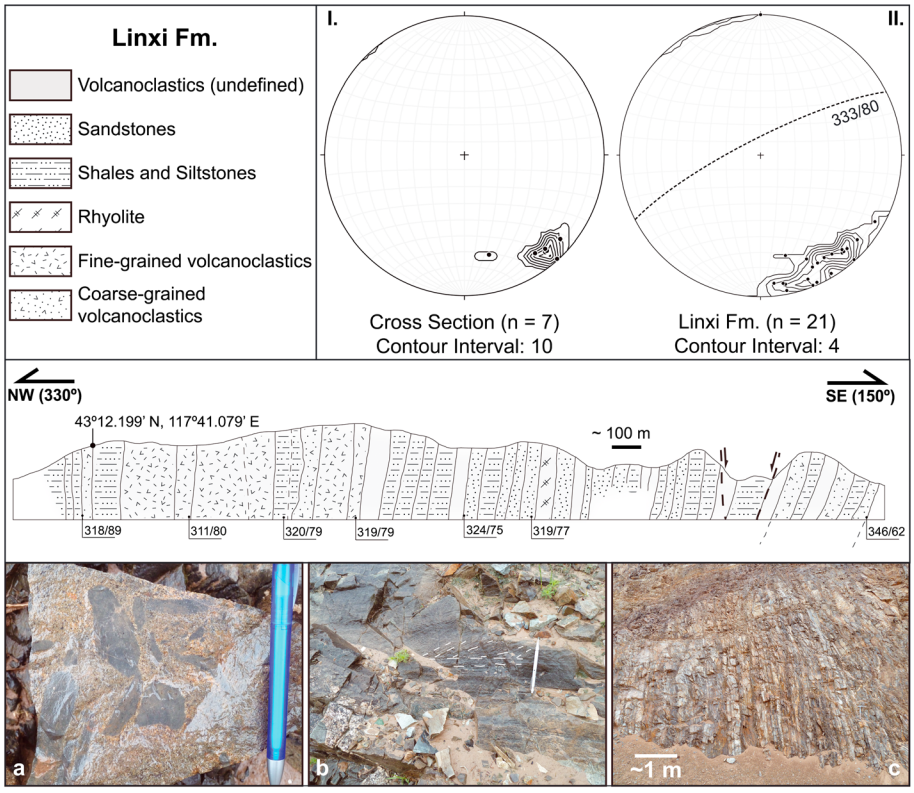

Figure 7. A cross section of turbiditic sequences with structural attitudes (dip azimuth/dip) in the Linxi Formation. Photographs show (a) conglomeratic arkose, (b) signs of cross-stratification in greywackes, and (c) vertical bedding of fine-grained turbiditic succession. Stereonets show (I.) measurements of S_0 from the cross section and (II.) measurements of S_0 from the Linxi Formation in the entire study area. The average of all measurements is projected as dashed great circle.

sample was from a felsic dike intruding a turbiditic succession of the Huanggangliang Formation, and one sample from an andesitic pyroclastic rock. Samples were first crushed, sieved, and milled and then separated by standard heavy liquid and electromagnetic techniques, followed by handpicking of zircons from the heavy liquid residue. Individual grains were randomly selected and mounted on double-sided adhesive tape under a binocular microscope. Grains were then embedded in epoxy resin and polished down to about half the grain size to reveal internal grain surfaces and structures. Sample mounts were photographed in reflected and transmitted light. In order to guide laser ablation isotope analysis, grain growth structures were later depicted as cathodoluminescence (CL) images (Figure 9).

U-Pb zircon ages were obtained using an LA-ICP-MS housed at the State Key Laboratory of Ore Deposit Geochemistry, Institute of Geochemistry, Chinese Academy of Sciences, Guiyang. A GeoLasPro laser ablation system (Lamda Physik, Göttingen, Germany) and an Agilent 7700x ICP-MS (Agilent Technologies, Tokyo, Japan) were combined for the experiments. The 193 nm ArF excimer laser, homogenized by a set of beam delivery systems, was focused on the zircon surface with an energy flux of 10 J/cm^2. Ablation protocol employed a spot diameter of 32 μm at 6 Hz repetition rate for 40 s (equating to 200 pulses) for most samples.

Figure 8. (a) Permian sedimentary strata unconformably overlain by horizontal Jurassic basalts on the southern bank of the Xar Moron River. (b) A felsic dike cross-cutting the Huanggangliang Formation.

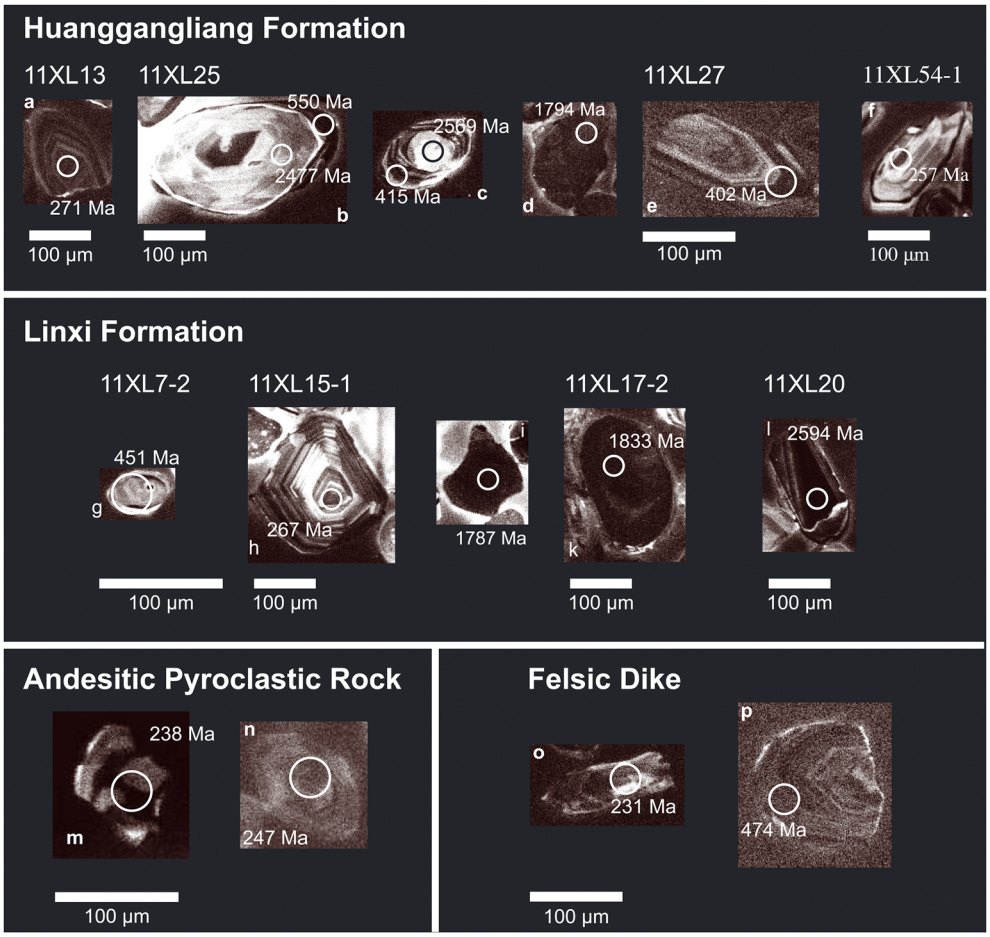

Figure 9. Representative CL images of zircons from the Huangganglang and Linxi Formations. Open circles (32–40 μm) show laser ablation analytical sites, and each spot is labeled with its individual $^{206}Pb^*/^{238}U$ or $^{207}Pb^*/^{206}Pb^*$ age (Ma), respectively.

A few zircon grains were ablated with a spot diameter of 40 μm. Helium was used as a carrier gas to efficiently transport aerosol to the ICP-MS.

Zircon 91500 ($^{207}Pb^*/^{206}Pb^*$ age of 1065.4 ± 0.3 Ma, $^{206}Pb^*/^{238}U$ age of 1062.4 ± 0.4 Ma) [*Wiedenbeck et al.*, 1995] was used as an external standard to correct for elemental fractionation, while zircon GJ-1 ($^{207}Pb^*/^{206}Pb^*$ age of 608.53 ± 0.37 Ma) [*Jackson et al.*, 2004] and Plešovice ($^{206}Pb^*/^{238}U$ age of 337.13 ± 0.37 Ma) [*Sláma et al.*, 2008] were used for quality control. Lead concentration in zircon was externally calibrated against NIST SRM 610 with Si as an internal standard, whereas Zr served as an internal standard for other trace elements [*Hu et al.*, 2011]. Data reduction was performed off-line by ICPMSDataCal [*Liu et al.*, 2010a, 2010b]. Weighted mean average ages of the youngest age peaks in sample 11XL14-2 (felsic dike) and 11XL24-1 (andesitic pyroclastic rock) were calculated using Isoplot 3.75 [*Ludwig*, 2008]. Geochronological results are provided in the supporting information Tables S1–S3.

A minimum of 90 zircon grains were analyzed for each sample. As outlined by *Vermeesch* [2004] 117 analyses are required to identify at a 95% confidence level every age component comprising more than 5% of the entire age population. According to *Andersen* [2005], 60 analyses per sample are sufficient to identify on a 95% confidence level a single age component representing more than 5% of the entire age population based on the standard binomial probability formula [*Dodson et al.*, 1988]. Both statements refer to the analysis of concordant ages. The total number of analyses undertaken in this study (1010 concordant ages), therefore, indicates that the probability of missing a single age population occurring in the region statistically tends to zero [see also *Andersen*, 2005]. Age histograms and concordia plots were produced by an in-house code using the Matlab environment provided by Mathworks® (Figures 5, 10–13, and 16; Matlab scripts and functions are

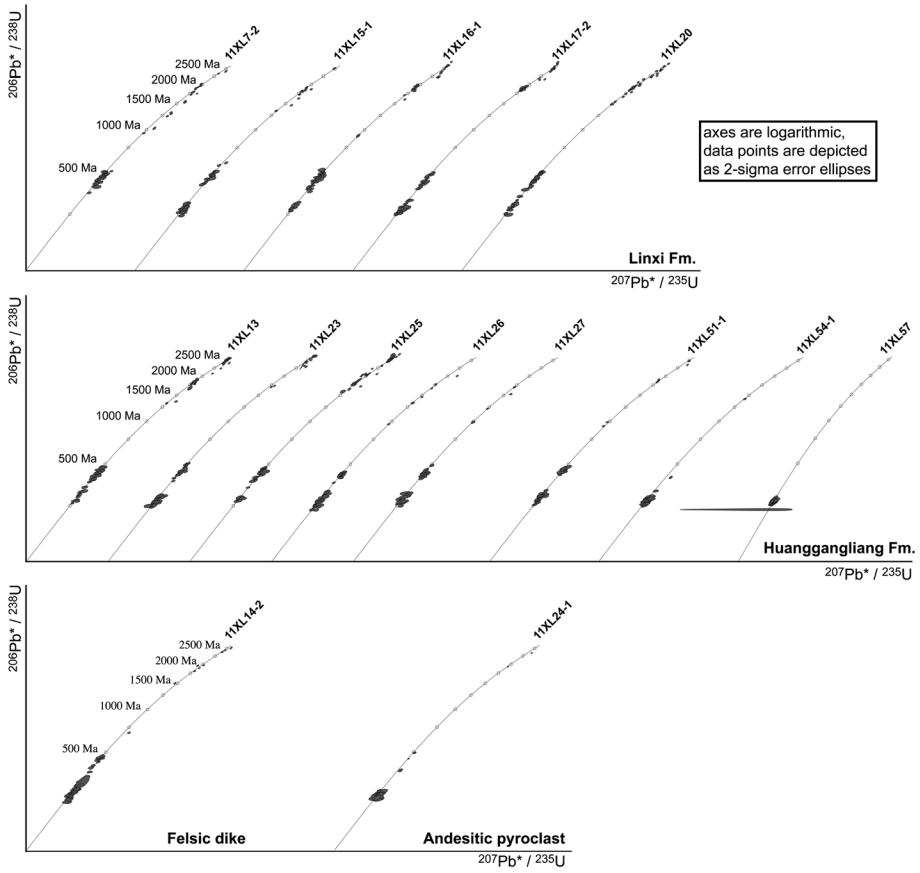

Figure 10. Zircon U-Pb concordia diagrams for detrital zircons from the studied samples collected from the Huangganglang and Linxi formations.

available upon request). The total age probability density distribution of each sample was calculated by assuming a Gaussian error distribution for each single age and its respective 1σ error. Single age probability density distributions were summed to obtain the probability density distribution of the sample, and then normalized by the number of total analyses of each sample. If ages are higher than 1 Ga, the age recorded by the $^{207}Pb^*/^{206}Pb^*$ ratio was selected; otherwise, the $^{206}Pb^*/^{238}U$ age was used. The concordia plots use a log-log scale in order to adequately visualize the entire age spectrum of a sample in a single plot. The unlikeliness that errors of each of the two isotope ratios reach simultaneously their maximum value has been taken into account by drawing error ellipses based on a 95% confidence level (2σ). In order to provide an additional measure to compare different probability density distributions quantitatively, a heterogeneity (H_{rel}) value has been calculated [*Pelto*, 1954; *Smosna et al*., 1999; *Sircombe*, 2004]. Probability density distributions with lower relative heterogeneity values tend to be dominated by fewer age peaks, and vice versa. The relative heterogeneity H_{rel} is defined as follows:

$$H_{rel} = 100\left(\frac{H}{H_{max}}\right)$$

with H describing the absolute value of heterogeneity using the information function [*Shannon and Weaver*, 1963; *Pelto*, 1954] for a data set consisting of n components and probability p_i of the ith age component:

$$H = -\sum_{i}^{n} p_i \ln\ p_i$$

and H_{max} describing the maximum value of H assuming equal probability of each occurring age component [*Pelto*, 1954; *Smosna et al.*, 1999]:

$$H_{max} = -n\left(\left(\frac{1}{n}\right)\cdot \ln\left(\frac{1}{n}\right)\right)$$

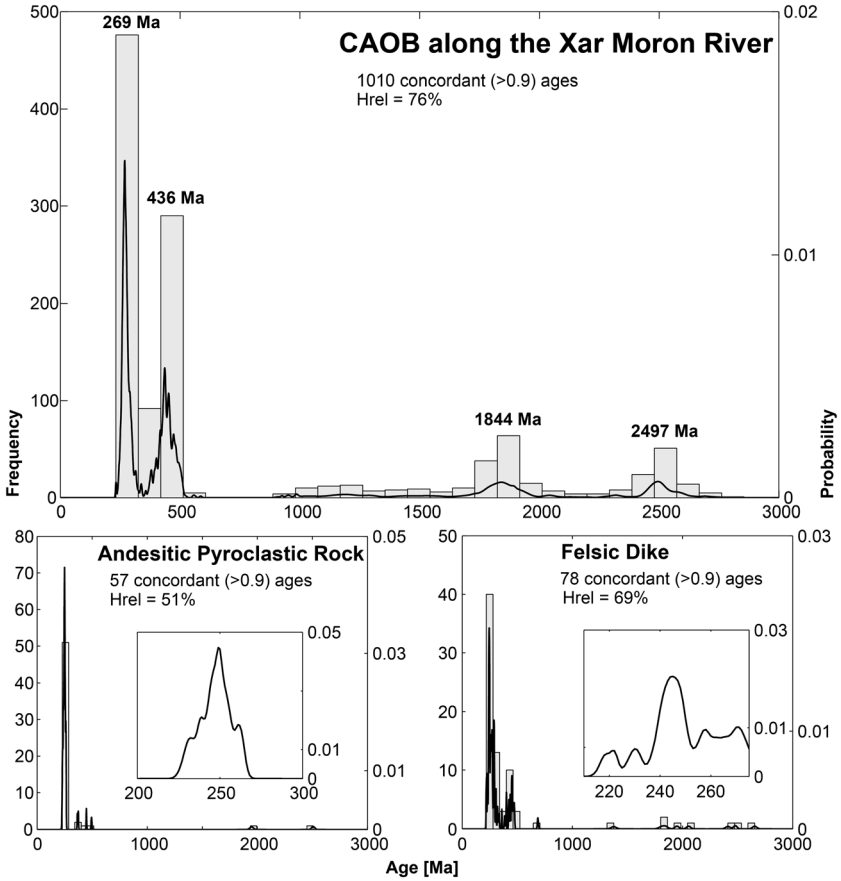

Figure 11. (a) Age distribution diagram for all detrital zircons from the Huanggangliang and Linxi formations in the Xar Moron River region. (b) Age distribution diagram for zircons from an andesitic pyroclastic rock. Inset shows probability distribution of the suggested age range of rock formation. (c) Age distribution diagram for zircons from a felsic dike crosscutting the Huanggangliang Formation. Inset shows probability distribution of the suggested age range of dike emplacement.

The heterogeneity values calculated are based on a 4000-component system for each sample, referring to an age range from 0 to 4000 Ma in 1 Ma steps. The large number of analyses undertaken in this study may indicate that changes of relative heterogeneity calculated for large data sets (e.g., all ages obtained in a rock formation) reflect changes in the sedimentary system.

Total percentage amount of quartz grains, feldspar grains, and lithic fragments of the volcanoclastic siltstone and sandstone samples (Figure 14) was obtained by the Gazzi-Dickinson counting method [*Dickinson*, 1985]. A minimum of 300 grains were systematically identified on each thin section and classified as quartz grain, feldspar grain, or lithic fragment (see supporting information Table S4). Percentages were plotted on a Quartz-Feldspar-Lithics (QFL-) ternary diagram (Figure 14) after *Dickinson* [1985]. Point-counting results are provided in the supporting information Table S4.

Major oxides were determined by wavelength-dispersive X-ray fluorescence spectrometry (XRF) on fused glass beads using a Rigaku RIX 2000 X-ray fluorescence spectrometer (XRF) at the Guangzhou Institute of Geochemistry, Chinese Academy of Sciences. Calibration lines used in quantification were produced by bivariate regression of data from 36 reference materials encompassing a wide range of silicate compositions [*Li et al.*, 2006], and analytical uncertainties are 1–5%. Results are presented in Figure 15 and supporting information Table S5.

4. Results

4.1. Geochronology

Concordant ages (>0.9 concordance between the $^{206}Pb^*/^{238}U$ and $^{207}Pb^*/^{235}U$ ratios) were plotted as combined histogram/probability density distribution plots (Figures 5, 11–13, and 16). Major age populations

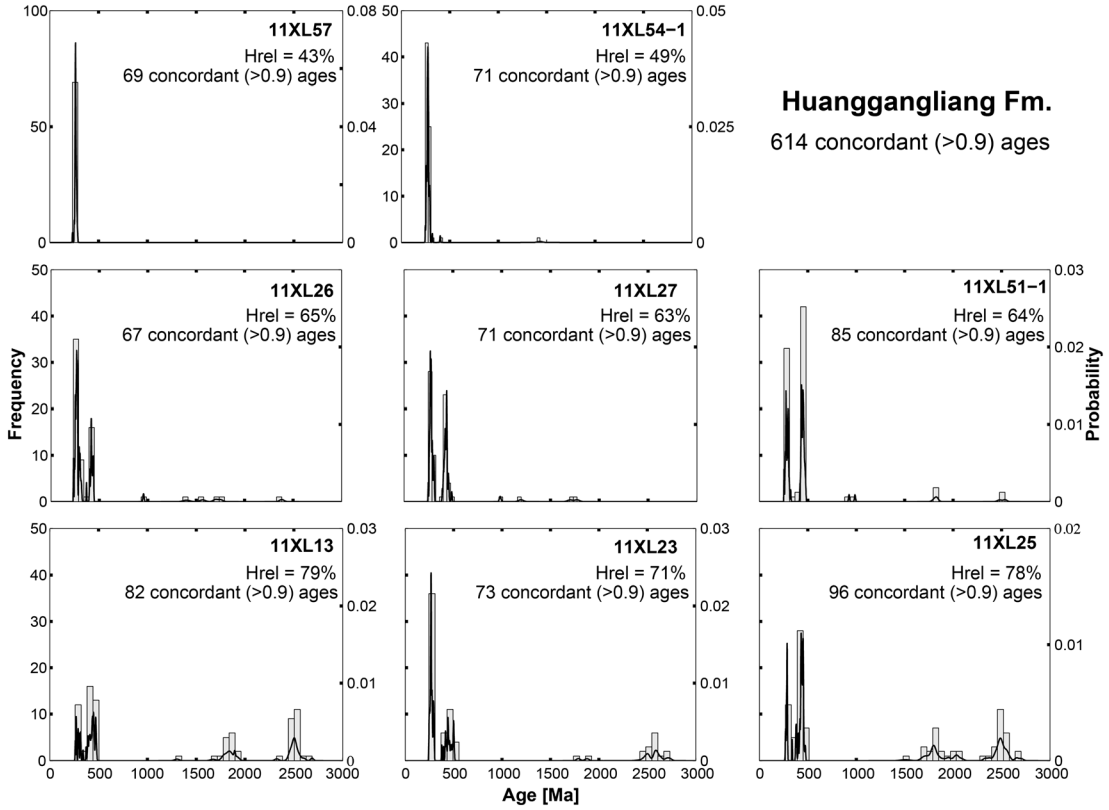

Figure 12. Age distribution diagrams for samples from the Huangganglíang Formation.

of all 1010 concordant ages are located at ~2497 Ma, ~1844 Ma, ~436 Ma, and ~269 Ma, with some Mesoproterozoic to Neoproterozoic ages but without any Archean ages (Figure 11). The overall value of relative heterogeneity (H_{rel}) is 76%. An age gap is identified between ~1000 Ma and ~500 Ma. Major Paleozoic age peaks are very distinct, separated by a narrow age gap at ~300 Ma.

4.1.1. Huangganglíang Formation

Concentric oscillatory zoning dominates the growth structure of most zircons throughout the samples (Figures 9a and 9f). Metamorphic overgrowths are rare but occur in sample 11XL25 (Figure 9b). Few zircon

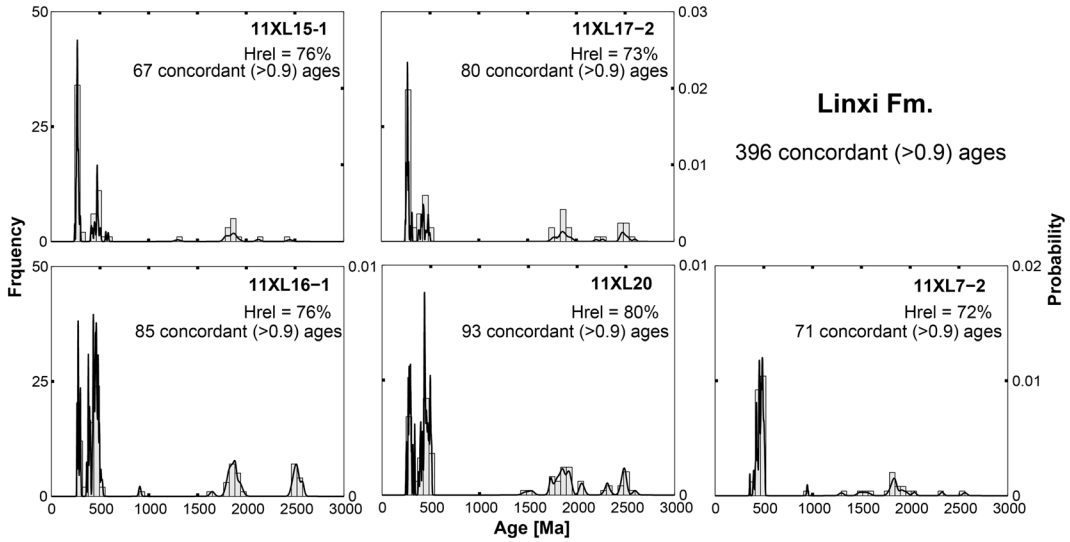

Figure 13. Age distribution diagrams for samples from the Linxi Formation.

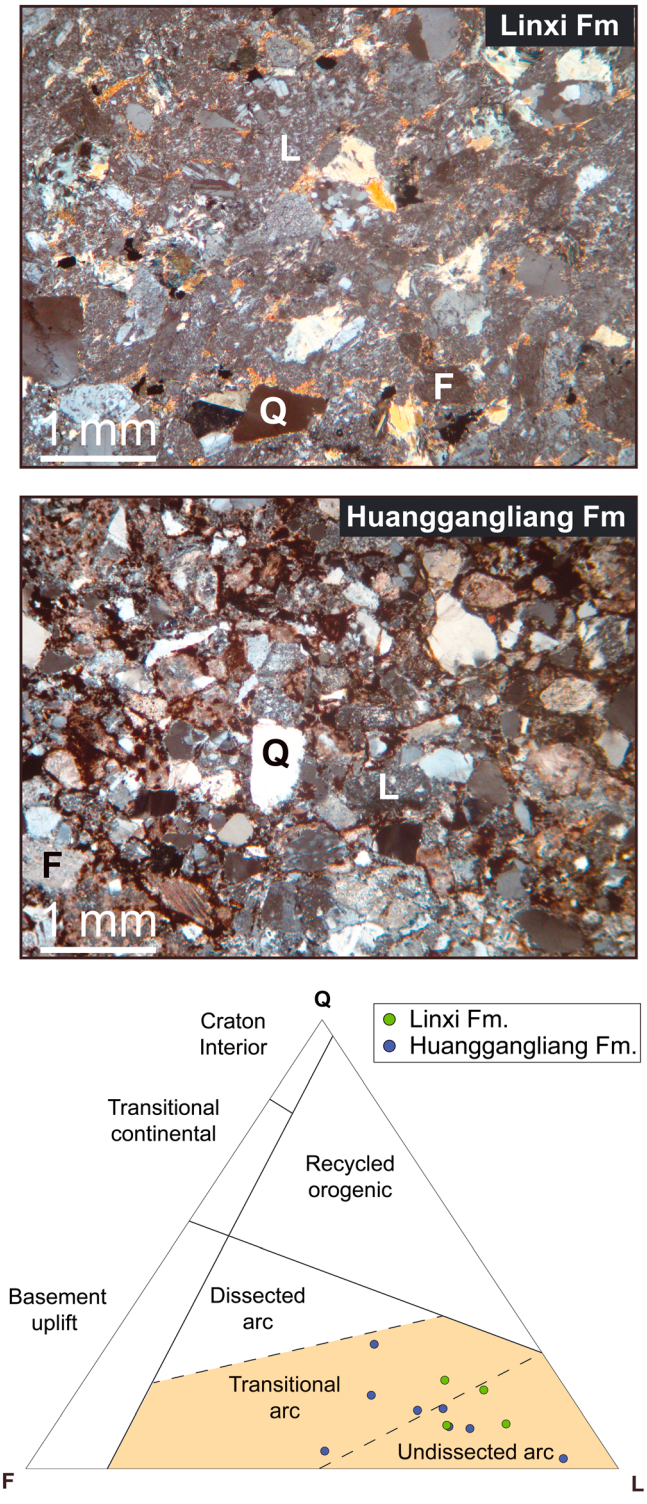

Figure 14. Photomicrographs showing representative textures of greywackes from the Huangganglang and Linxi Formations and Quartz-Feldspar-Lithics (QFL) diagram with point-counting results.

grains contain inherited Precambrian aged cores with younger oscillatory rim (Figure 9c). Zircons without any visible internal structures occur, but are rare (e.g., Figure 9d) and can be explained by either a comparatively high U-content or a metamorphic origin. However, the CL image quality should be taken into account here. Zircon grains are generally euhedral to subhedral (Figure 9e), with a few subrounded grains (Figures 9b and 9c), indicating a higher degree of reworking, particularly in sample 11XL25. Analytical sites show a range of Th/U ratios from 0.03 to 0.65; most, however, are above 0.07. The majority of zircons are, therefore, of magmatic origin, and only a few underwent metamorphism or reworking.

Overall, four age groups can be observed in the formation: ~2.50 Ga, ~1.80 Ga, ~437 Ma, and ~268 Ma (Figure 12). The value of relative heterogeneity of the entire formation is $H_{rel} = 72\%$ (Figure 4), indicating the dominance of several age groups; however, they are not consistently present throughout the Huangganglang Formation. Samples 11XL57 and 11XL54-1 are dominated by a single age peak at ~268 Ma. This is also reflected in low values of relative heterogeneity ($H_{rel} = 43\%$ and $H_{rel} = 49\%$), indicating the dominance of the one age group. Samples 11XL26, 11XL27, and 11XL51-1 mainly contain the ~268 Ma and ~437 Ma age groups, with minor Precambrian ages, if present at all. The values of relative heterogeneity are higher ($H_{rel} = 65\%$ and $H_{rel} = 63\%$). In contrast, samples 11XL13, 11XL23, and 11XL25 contain all age groups. Their value of relative heterogeneity are the highest, with $H_{rel} = 79\%$, $H_{rel} = 71\%$ and $H_{rel} = 78\%$, respectively.

4.1.2. Linxi Formation

In general, zircons from the samples show concentric oscillatory zoning (Figure 9h). A larger number of grains have metamorphic rims (Figures 9g and 9k). Few do not have any visible internal structures (Figure 9k) and are either light colored (Figure 9g) or dark under cathodoluminescence (Figure 9i). However, the CL image quality is relatively poor and might lead to some

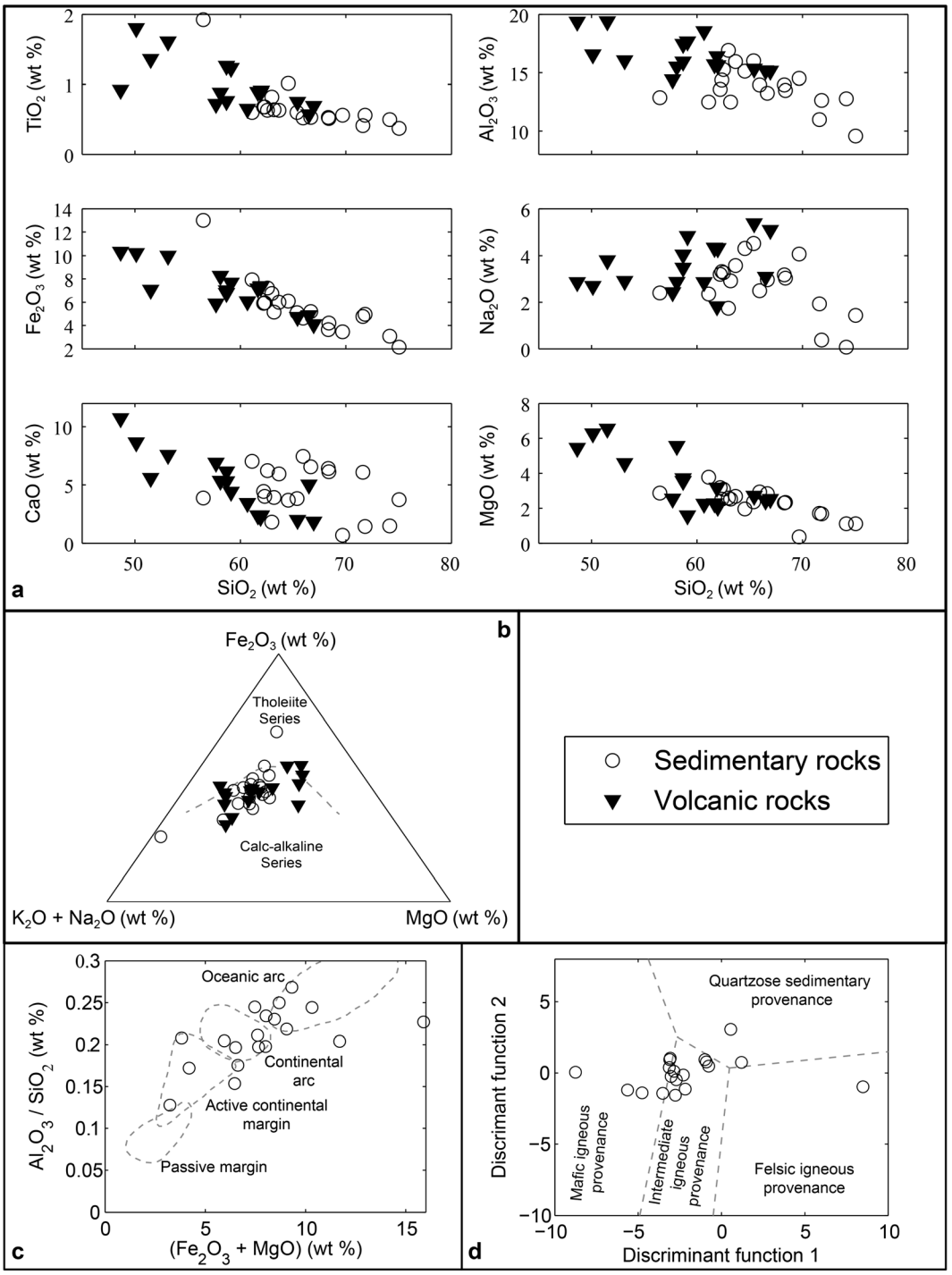

Figure 15. (a) Harker variation diagrams of major elements for volcanic and sedimentary rocks in the study region. (b) AFM diagram. (c) A bivariate plot of (Al_2O_3/SiO_2) versus (Fe_2O_3/MgO) [*Bhatia*, 1983]. (d) A discriminant function diagram after *Roser and Korsch* [1988]. The discriminant functions are discriminant function 1 = 30.638 TiO_2/Al_2O_3 − 12.541 Fe_2O_3/Al_2O_3 + 7.329 MgO/Al_2O_3 + 12.031 Na_2O/Al_2O_3 + 35.402 K_2O/Al_2O_3 − 6.382 and discriminant function 2 = 56.500 TiO_2/Al_2O_3 − 10.879 Fe_2O_3/Al_2O_3 + 30.875 MgO/Al_2O_3 − 5.404 Na_2O/Al_2O_3 + 11.112 K_2O/Al_2O_3 − 3.89.

bias. The degree of rounding is highly variable ranging from euhedral crystals (e.g., Figure 9h) to well-rounded grains (Figures 9k and 9l). A small number of grains show striped zoning originating either from (a) reworking of larger concentric oscillatory grains or (2) from crystallization from mafic magma (Figure 9l). All laser ablation sites show a large range of Th/U ratios from 0.03 to 2.02, with most above

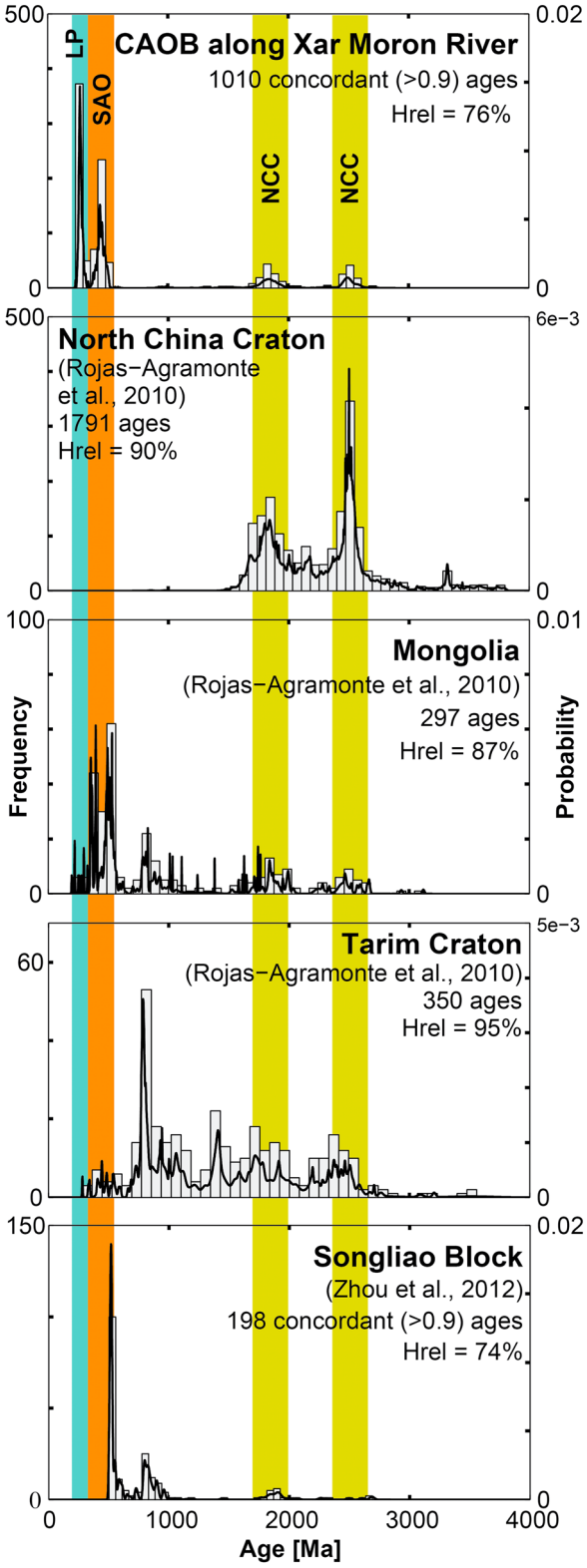

Figure 16. Comparison of the age population of the Permian sedimentary successions (Huanggangliang and Linxi Formations) with those of major regional provenance terranes in the region. LP: Late Permian; SAO: Southern Accretionary Orogen; NCC: North China Craton.

0.07. This indicates that most zircons from the samples are of magmatic origin, though a small number of grains underwent metamorphic growth either as rims or single zircons.

Age populations recognized in the samples of the Linxi Formation are similar to those of the Huanggangliang Formation: ~2.49 Ga, ~1.85 Ga, ~455 Ma, and ~270 Ma (Figures 5 and 13). These age groups are relatively well represented in all samples, in contrast to the Huanggangliang Formation (Figure 12). The overall value of relative heterogeneity (H_{rel} = 79%) is higher as well (Figure 5). The four age groups are all present in samples 11XL17-2, 11XL20, and 11XL16-1 as also indicated by the highest values of relative heterogeneity in these (H_{rel} = 73%, H_{rel} = 80%, and H_{rel} = 76%, respectively; Figure 13). In comparison, Precambrian zircons are less represented in sample 11XL15-1 but still occur, as also demonstrated by a lower value of relative heterogeneity (H_{rel} = 68%; Figure 13). Sample 11XL7-2 is the only sample with no pronounced ~270 Ma age peak (H_{rel} = 72%), although a few discordant zircons around ~270 Ma were measured.

4.1.3. Andesitic Pyroclastic Rock and Felsic Dike

Sample 11XL24-1 is an andesitic pyroclastic rock. Zircons are generally euhedral to subhedral and predominantly exhibit concentric oscillatory zoning (Figure 9n). A significant amount of zircon grains show patchy zoning (Figure 9m). Laser ablation sites show a range of Th/U ratios from 0.10 to 1.65, with an average value of 0.58. Analyzed zircons are, therefore, of magmatic origin. A dominant single age peak is located between ~225 Ma and ~275 Ma, which yielded an unrealistically precise weighted mean age of 249 ± 2 Ma (MSWD = 12; Figure 11). The high MSWD indicates a large component of geological scatter in the data, most likely due to the presence of several similar age populations. The sample might have been multiply reworked, and pyroclastic material successively added before final deposition. The older zircon grains are considered to be xenocrysts captured either from the nearby Permian volcanic arc rocks or volcanoclastic strata during magma ascent. Thus, we refrain from making use of the weighted mean age.

The majority of the youngest ages suggest that the andesitic pyroclastic rock formed at a later time, most likely between the Early to Middle Triassic.

Sample 11XL14-2 was taken from a felsic dike (Figure 8b), which intrudes the Huanggangliang Formation turbidites. It crosscuts the overall bedding structure of the host rock at a low angle with respect to the original bedding. Most zircons from the sample are euhedral to subhedral (Figure 9o) with mostly concentric oscillatory zoning (Figure 9p). Laser ablation sites show Th/U ratios from 0.16 to 1.13, with an average value of 0.83, and the grains are, therefore, considered to be of magmatic origin. However, a few grains do not show any zoning or are slightly rounded, and they are likely to be xenocrysts captured either (1) from the host rock or (2) during magma ascent. A dominant group of zircons is located between ~255 Ma and ~245 Ma, which gave a weighted mean average age of 242 ± 3 Ma (MSWD = 9.6; Figure 11), slightly younger than that calculated for the andesitic pyroclastic rock (11XL24-1). The high MSWD indicates a large component of geological scatter and probably the presence of several similar age populations. This can be understood by assuming that captured zircons from the nearby volcanic and sedimentary strata were added during dike emplacement, thus possibly tapping several age reservoirs. As discussed above, the Huanggangliang Formation, in where the dike intruded, is characterized by age peaks at ~2.49 Ga, ~1.85 Ga, ~455 Ma, and ~270 Ma. These ages all occur in the age population of the felsic dike. Other zircons mostly yielded ages around ~451 Ma, with a few yielding Precambrian ages ranging from 2656 ± 19 Ma to 1376 ± 23 Ma. The Early to Middle Triassic volcanic activity, evidenced by the andesitic pyroclastic rock, also contributed zircons, adding to the complexity of the age distribution. Since these ages are not considered in the calculation of the weighted mean average age, the latter only can serve as a general age reference for the location of the major age population in the dike. Based on the youngest zircon age groups, it is, thus, assumed that dike emplacement occurred later, between the Early to Middle Triassic.

4.2. Major Element Analysis

Variations of major elements of various sedimentary and volcanic rock suites occurring in the study region are depicted as Harker and AFM diagrams (Figures 15a and 15b). Generally, TiO_2, Al_2O_3, Fe_2O_3, and MgO decrease with increasing SiO_2 independent of rock type. This trend is less visible for Na_2O and CaO over SiO_2, which might be the result of chemical alteration due to weathering. Nevertheless, the sedimentary rock suite is overall situated toward higher quartzose content and less detrital content (e.g., feldspars and volcanic rock fragments). The volcanic rock suite is effectively the opposite. Oxides plotted on the AFM diagram have revealed a generally calc-alkaline subduction-related tectonic environment [*Li*, 2006; *Zhang et al.*, 2007; *D. P. Li et al.*, 2011; *Y. L. Li et al.*, 2011a; *Han et al.*, 2012] (Figure 15b). However, the location of data points varies largely. Discrimination plots according to *Bhatia* [1983] and *Roser and Korsch* [1988] (Figures 15c and 15d, respectively) further indicate (1) an overall arc setting and (2) a dominantly intermediate to mafic igneous provenance of the sediments, which suggests that the volcanic arcs are a principal source. A certain degree of sedimentary reworking until final deposition is indicated by the higher mineralogical maturity of the sedimentary rock suite compared to the volcanic rock suite. In summary, a very complex arc setting with generally short sedimentary transport distances in a tectonic convergent setting is recognized.

4.3. Field, Compositional, and Textural Observations

The collected samples from the Huanggangliang Formation cover a broad spectrum of volcanoclastic sedimentary rocks (greywackes and sandstones). In comparison, samples from the Linxi Formation (greywackes and sandstones) are texturally and compositionally more mature.

Dip and strike measurements of sedimentary strata of the Huanggangliang and Linxi Formations show an average southwest-northeast striking of subvertical beds (Figures 6 and 7) corresponding well with regional tectonic features such as major regional faults (e.g., the Linxi Fault).

Percentage amounts of quartz grains, feldspar grains, and lithic fragments obtained by point counting on thin sections suggest a transitional to undissected arc setting (Figure 14). Percentages of lithic fragments mostly are above 60% per sample suggesting dominantly short sedimentary transport distances.

4.3.1. Huanggangliang Formation

A detailed cross section through the Huanggangliang Formation reveals extensive meter-scale folding. Folds are mostly upright, with a few being isoclinal (Figure 6). Those folds are accompanied by local thrust faults of various orientations and of unknown age. The presence of small-scale shear folds further confirms tectonic

stress accommodation by thrusting and shearing (Figure 6c). Local rotational features associated with dragged beds further indicate a constant compressional tectonic environment. Structural attitude measurements from the formation in the entire study area reveal a large variation of orientations due to its extensive deformation. A preferred fold vergence as possible indicator for subduction polarity was not observed. Instead, fold axes seem to strike roughly southwest-northeast with varying inclination of fold vergence. However, the overall average southwest-northeast strike of the formation is in accordance with the orientation of large-scale tectonic features such as the regional Linxi or Xar Moron Faults. Thus, the Huangganglіang Formation appears to have been subjected to major southeast-northwest shortening in a convergent setting after its deposition.

4.3.2. Linxi Formation

Deformational features in the Linxi Formation (Figure 7) are not as distinct as those in the Huangganglіang Formation (Figure 6). Meter-scale folding within the Linxi Formation was not observed. However, larger-scale regional folding may have occurred but was not detected in this study and needs further investigation. Exposed along the cross section are relatively homogeneous and vertically bedded volcanoclastic strata striking southwest-northeast (see stereonets in Figure 7).

5. Discussion

5.1. Provenance Terranes

Provenance analysis of Late Paleozoic sedimentary arc basins along the Xar Moron River can provide an important insight into the role of major tectonic units as sedimentary provenance terranes during the final closure of the Paleo-Asian Ocean along the Solonker Suture Zone. Their relative contributions can be identified and defined by their characteristic age probability density distributions (Figure 16) [*Sircombe*, 2004; *Gehrels et al.*, 2011]. Their paleogeographic location, as an indirect measure for the direction of regional sediment transport toward the arc basins, may also serve as an indicator of subduction polarity in tectonic convergent settings.

The North China Craton in the south and the Mongolian arcs in the north represent the most likely provenance terranes due to their close geographic location to the study region. Other provenance terranes such as the Siberian Craton, the Tarim Craton, Gondwana-derived fragments within the CAOB, and a Pan-African orogenic terrane located in northeast China [*Zhou et al.*, 2012] are less likely to have influenced the sedimentary system in the study region and will only be briefly discussed here. A detailed geochronological summary and discussion of most of these provenance terranes have been provided by *Rojas-Agramonte et al.* [2011, and references therein].

The Paleoproterozoic age peaks (~2497 Ma and ~1844 Ma) detected in the Xar Moron River region in this study are similar to those from the North China Craton [e.g., *Darby and Gehrels*, 2006]. According to *Rojas-Agramonte et al.* [2011], zircon U-Pb ages originating from the North China Craton generally range from ~3.8 Ga to ~1.6 Ga, with major age peaks at 2.8–2.6 Ga, 2.4–2.35 Ga, and 2.1–1.85 Ga. Taking into account the proximity to the study region, the North China Craton is identified as a significant provider of sedimentary detritus to the Huangganglіang and Linxi Formations.

The Mongolian arcs comprise a large variety of Paleoproterozoic to Paleozoic zircon U-Pb ages. Major age peaks are around 2710–2182 Ma, 2060–1820 Ma, 950–760 Ma, 580–460 Ma, and 400–340 Ma. These ages were sourced from the arc terranes themselves and the Tarim Craton, while the North China Craton is not considered as a contributor [*Rojas-Agramonte et al.*, 2011]. The large value of relative age heterogeneity of the Mongolian arcs ($H_{rel} = 87\%$) cannot be observed in the age population in this study ($H_{rel} = 75\%$). Prominent Mongolian Neoproterozoic, as well as Earliest Paleozoic (~515 Ma), age populations were not detected in this study. Therefore, the Mongolian arcs as a whole can only be accounted a minor role as a provenance terrane, if at all. However, it remains unclear whether independent single units of the Mongolian arcs contributed to the Early Paleozoic and minor Mesoproterozoic to Neoproterozoic age populations found in the study region.

The Siberian Craton is characterized by a larger population of Archean to Early Paleoproterozoic ages [*Rojas-Agramonte et al.*, 2011]. Taking into account the paleogeographic distance and the late final eastern attachment to the CAOB after the Late Jurassic/Early Cretaceous closure of the Mongol-Okhotsk Ocean [e.g., *Cogne et al.*, 2005], the Siberian Craton is unlikely to have contributed detritus to the study region. The Tarim

Craton reveals a very heterogeneous age distribution ($H_{rel} = 95\%$) with a distinct Neoproterozoic population (~788 Ma), neither of which is observed in the study area. Recently, *Ge et al*. [2013] reported abundant 2.5 Ga and 1.85 Ga ages, similar to those of the North China Craton. However, we discard the Tarim Craton as being an age source, though *Rojas-Agramonte et al.* [2011] suggested that it was an important contributor of detrital material to the Paleozoic basins in Mongolia. Large-scale northeastern Gondwana-derived fragments in the eastern CAOB, which could have provided detritus to the study region, are not reported so far. As pointed out by *Rojas-Agramonte et al.* [2011], Gondwanan fragments are generally characterized by a Pan-African age peak (650–550 Ma) and a Mesoproterozoic age gap (~1.75–1.0 Ga). These age peak and gap are absent in the analyzed samples in this study. They, thus, are not considered as provenance sources of the Permian sedimentary basins along the Xar Moron River. However, e.g., *Zhou et al.* [2012] and *Han et al.* [2012] proposed that the Erguna, Xing'an, Jiamusi-Khanka, and Songliao blocks in northeast China have Pan-African basement and represent fragments that rifted from northern Gondwana, and may have influenced sedimentary systems in the region during Late Paleozoic.

Therefore, other source terranes need to be considered to explain the dominant occurrence of Early and Late Paleozoic age populations (~436 Ma and ~269 Ma, respectively) detected in the study area. An Early Paleozoic arc along the northern margin of North China existed [*Xiao et al.*, 2003], termed the Southern Accretionary Orogen ("Southern Orogen") by *Jian et al.* [2008, 2010]. Early Paleozoic activity and collision with a microcontinent (Hunshandake microcontinent) along the Ondor Sum Subduction-Accretion Complex were recently reported [*Shi et al.*, 2013; *Xu et al.*, 2013]. Phengites in blueschists from the Ondor Sum Subduction-Accretion Complex gave Ar/Ar ages of 453.2 ± 1.8 Ma and 449.4 ± 1.8 Ma [*de Jong et al.*, 2006]. Zircons from a biotite-plagioclase gneiss sample collected from the Xilinhot Complex yielded upper and lower intercept ages of 437 ± 3 Ma and 316 ± 3 Ma, respectively [*Shi et al.*, 2003]. However, the affinity of the Xilinhot Complex with the Southern Accretionary Orogen is not clear, and it might be closer related to the Northern Accretionary Orogen. Additionally, *Cope et al.* [2005] considered that a continental arc existed along the northern margin of the North China Craton from ~400 to ~275 Ma based on detrital zircon analysis of Carboniferous to Permian nonmarine strata. These lines of evidence suggest that the Early and Late Paleozoic zircons in the arc basins originated most likely from a major Paleozoic provenance terrane along the northern margin of North China, not from the Mongolian arcs, which were on the opposite northern edge of the Paleo-Asian Ocean.

In summary, we consider that at least two provenance terranes contributed to the Permian arc basins along the Xar Moron River: (1) the Precambrian basement of the North China Craton in the south and (2) the Southern Accretionary Orogen along the northern margin of North China. The presence of a few Mesoproterozoic to Neoproterozoic zircons in the study area may indicate the involvement of a recently discussed microcontinent (Hunshandake microcontinent) [*Shi et al.*, 2013; *Xu et al.*, 2013]. A number of Late Paleozoic ages may also have been contributed to the arc basins by the active Northern Accretionary Orogen during the final stages of ocean closure. However, their contribution to the Late Permian age population would be indistinguishable from those of the Southern Accretionary Orogen. Furthermore, the detrital zircon age spectrum in this study is dominated by the Precambrian ages of the North China Craton and the Early Paleozoic ages of the Southern Accretionary Orogen. Since Carboniferous ages should commonly occur within the Northern Accretionary Orogen (e.g., in the Xilinhot Complex) [*Shi et al.*, 2003], its influence during formation of the Linxi and Huanggangliang Formations appears insignificant. Whether Carboniferous ages can be found north of the study region in Late Permian formations closer to the Northern Accretionary Orogen needs to be further investigated.

5.2. Tectonic Setting During the Late Paleozoic

Available data suggest a tectonic convergent (oceanic subduction and continental collision) setting across the Solonker Suture Zone during the Permian. The location of the detected provenance terranes implies southward directed oceanic subduction beneath the Southern Accretionary Orogen and the North China Craton. The Permian age population coincides with the stratigraphic age of the host formation. The overall detrital zircon U-Pb age distribution of the study area, thus, resembles that of a convergent tectonic setting as recently characterized by *Cawood et al.* [2012], thus representing a basin environment within or near an active arc system. This is supported by arc-related volcanic rocks along the Xar Moron River, which are characterized by calc-alkaline compositions [*Li*, 2006; *Zhang et al.*, 2007; *D. P. Li et al.*, 2011; *Y. L. Li et al.*,

2011a; *Han et al.*, 2012]. In this study, we show that the Permian sedimentary and volcanic rock suites along the Xar Moron River are geochemically related (Figure 15). The sedimentary rock suite is characteristic of a higher quartzose but less detrital content compared with the volcanic rock suite. Nevertheless, a seamless geochemical trend toward higher silica content can be observed between both rock types. Geochemically, a mafic to intermediate sedimentary provenance terrane is suggested, consistent with an overall active arc setting in Permian. These observations suggest short transport distances from the major source regions and the sedimentary basins, with a certain degree of sedimentary reworking. This is further supported by the immaturity of the sedimentary (volcanoclastic) rocks (Figure 14). Although *Zhang et al.* [2008] recognized volcanic rocks around Xilinhot showing bimodal geochemical features, possibly due to formation in a post-collisional extensional setting, such bimodal-featured volcanic rocks are limited in the area. In addition, geochemical data show that granitoid rocks in the region show affinities to those in arcs or collisional belts [*Chen et al.*, 2000, 2009a]. Further evidence for an arc and/or collisional environment is the presence of paired metamorphic belts farther west of the study area, of which the high-pressure belt is represented by blueschists in the Ondor Sum Subduction-Accretion Complex [*Yan et al.*, 1989; *de Jong et al.*, 2006]. We assume that the Ondor Sum Subduction-Accretion Complex represents the northern accretionary wedge of the Baolidao Arc Accretion Complex. In addition, *X. H. Zhang et al*. [2009] recognized a suprasubduction-zone ophiolite suite close to the Erdaojing Complex north of the Xar Moron River along the Linxi Fault, which was previously considered to be a subduction-related orogenic belt [*Xu and Chen*, 1997; *Meng et al.*, 2010]. Furthermore, *Shi et al.* [2003] assumed a turbiditic fore-arc protolith for the Xilinhot metamorphic complex. As shown in Figure 14, point-counting results of samples in this study indicate a transitional to undissected arc setting. Distinction between different arc settings within the diagram is not clear, which supports the idea of a complex convergent tectonic setting during the Permian. In summary, a subduction and collisional tectonic environment is inferred across the present Xar Moron River area during the Late Paleozoic.

5.3. Timing of the Closure of the Paleo-Asian Ocean

The youngest major age peak observed in all sedimentary rock samples in the study area is at ~270 Ma (Figures 4 and 11–13), which defines the maximum depositional age of sedimentary rocks in the arc basins in which the Huanggangliang and Linxi Formations were deposited. An andesitic pyroclastic rock collected from the southern shoreline of the Xar Moron River (sample 11XL24-1; Figure 11) formed between the Early and Middle Triassic, interpreted as the timing of latest volcanic activity related to the southward subduction of oceanic lithosphere of the Paleo-Asian Ocean. An undeformed felsic dike (sample 11XL14-2, Figures 8b and 11) intruding the Huanggangliang Formation between the Early Triassic and Middle Triassic is interpreted to have recorded a period of latest magmatic activity and thus giving a constraint on the minimum depositional age of the Huanggangliang Formation. The dominant age peaks in both igneous rocks, however, are located in the Early Triassic (240–250 Ma). Taken together, our new data suggest that the final closure of the Paleo-Asian Ocean along the Solonker Suture Zone in the Xar Moron River area most likely occurred in the period between 240–270 Ma. This is consistent with previous data obtained in the Xar Moron River region [e.g., *Li et al.*, 2007; *Y. L. Li et al*., 2011b]. For example, magmatic zircons from a biotite-plagioclase schist and an intrusive syncollisional granite of the Shuangjing Complex located along the northern banks of the Xar Moron River yielded ages of 298 ± 2 Ma and 272 ± 2 Ma, respectively, suggesting that the final closure of the Paleo-Asian ocean has occurred at some time after 298 ± 2 Ma and 272 ± 2 Ma, not in the Early Paleozoic. In addition, previous structural, sedimentary, and geochronological data from other areas in vicinity of the Xar Moron River region also suggested that the Solonker Suture Zone developed in the Late Paleozoic or Early Triassic [e.g., *Xiao et al.,* 2003, 2009; *Li*, 2006; *Windley et al.*, 2007; *Jian et al.,* 2008, 2010], in accordance with the result of this study.

5.4. A Tectonic Scenario for the Solonker Suture Zone

Based on the above discussion about (a) major provenance terranes for the Permian arc basins along the Xar Moron River, (b) the tectonic setting during Paleozoic time, and (c) the timing of the final closure of the Paleo-Asian Ocean, we propose the following updated tectonic scenario for the Paleozoic evolution of the Solonker Suture Zone (Figure 17).

During Late Ordovician to Devonian time (Figure 17a), the Paleo-Asian Ocean lithosphere was subducted beneath the northern margin of North China, forming an Andean-type continental margin, called the

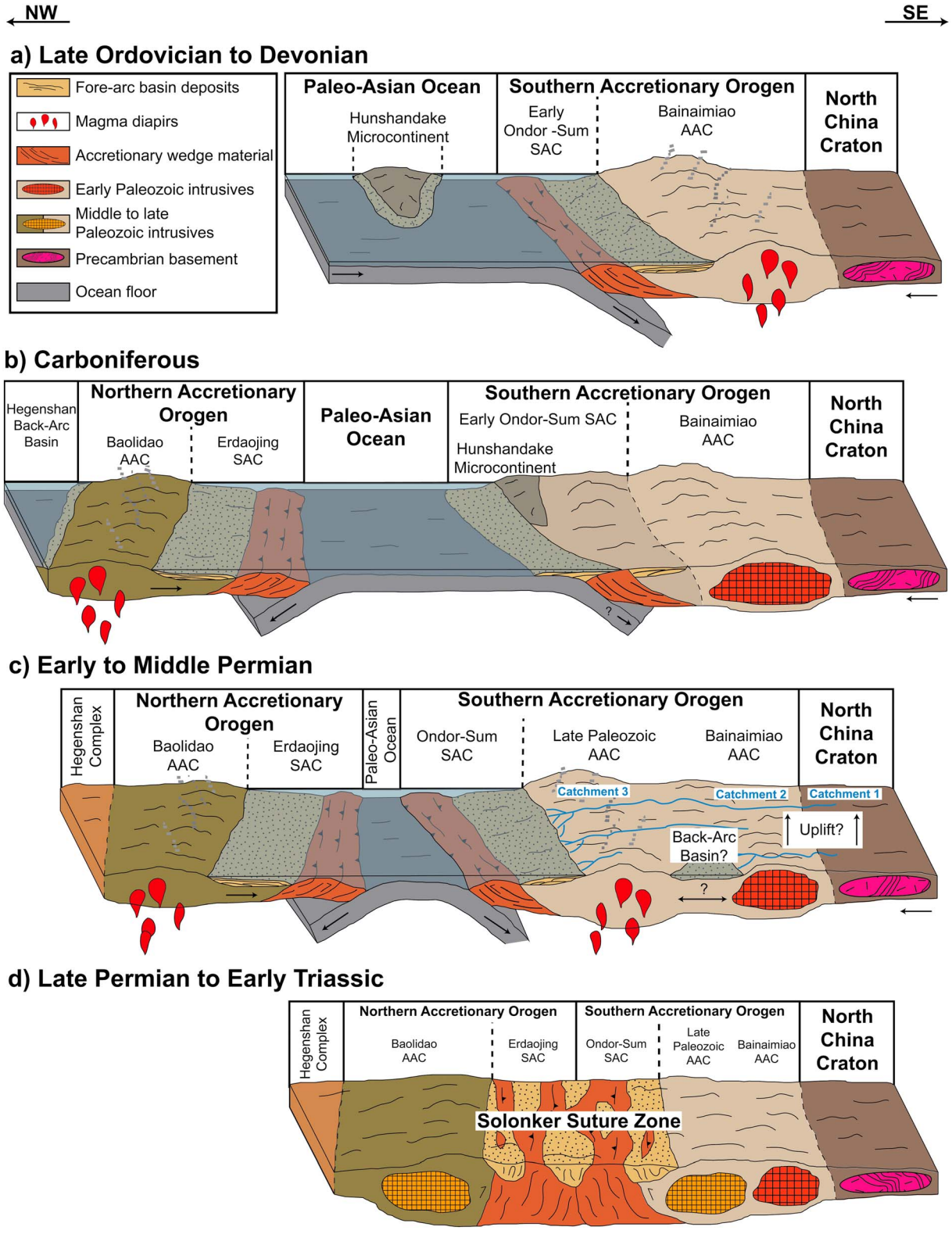

Figure 17. An updated scenario proposed for the tectonic evolution of the Solonker Suture Zone: (a) southward oceanic subduction beneath the Southern Accretionary Orogen and the North China Craton and approach of the Hunshandake Microcontinent during Late Ordovician to Devonian time; (b) docking of the Hunshandake Microcontinent onto the Southern Accretionary Orogen, cessation of subduction-related magmatic activity, and northward subduction beneath the Northern Accretionary Orogen during Carboniferous time; (c) final contraction of the Paleo-Asian Ocean due to double-sided subduction during Early to Middle Permian time; (d) final suturing during Late Permian to Early Triassic time. SAC: subduction-accretion complex; AAC: arc-accretion complex.

Southern Accretionary Orogen [*Jian et al.,* 2008, 2010]. The Southern Accretionary Orogen comprises the Bainaimiao Arc-Accretion Complex and the precursor of the Ondor Sum Subduction-Accretion Complex [*Xiao et al.*, 2003]. The Hunshandake Microcontinent is considered to be a microcontinental block within the Paleo-Asian Ocean, approaching the northern margin of North China [*Shi et al.*, 2013; *Xu et al.*, 2013].

In the Carboniferous (Figure 17b), northward intraoceanic subduction within the Paleo-Asian Ocean took place, forming a new accretionary orogen, called the Northern Accretionary Orogen, which is represented by the Baolidao Arc-Accretion Complex and the Erdaojing Subduction-Accretion Complex [*Xiao et al.*, 2003]. In the Late Carboniferous, subduction-related magmatism in the Southern Accretionary Orogen ceased, since few such-aged zircons are observed in the Permian arc basins, where the rocks of the Huanggangliang and Linxi Formations formed later. The Hunshandake Microcontinent most likely had accreted to the Southern Accretionary Orogen on the northern margin of North China at this stage [*Shi et al.*, 2013; *Xu et al.*, 2013], which might also explain temporary cessation of magmatic activity.

In the Early to Middle Permian (Figure 17c), the Paleo-Asian Ocean started to close due to double-sided subduction beneath both the Northern and Southern Accretionary Orogens [*Xiao et al.*, 2003]. This led to widespread arc magmatism as indicated by a major Late Paleozoic age peak in the Huanggangliang and Linxi formations. In addition, sediments in the arc basins situated within the Ondor Sum Subduction-Accretion Complex were also sourced from the Precambrian basement of North China and the Early Paleozoic arc rocks in the Southern Accretionary Orogen. In this period the Huanggangliang Formation formed, which was affected by significant folding and deformation while subduction continued. A complex arc environment, including opening back-arc basins, narrow ocean basins, and/or concurrent uplift of the hinterland, might be responsible for a complex sedimentary system. This would explain the inconsistent appearance of age populations in the sedimentary samples of the Huanggangliang Formation.

From the Late Permian to Early Triassic (Figure 17d), double-sided subduction led to the closure of the Paleo-Asian Ocean, resulting in collision between the Northern and Southern Accretionary Orogens, forming the intervening Solonker Suture Zone. The sedimentary rocks of the Linxi Formation were deposited in the latest existing arc basins during this period. These rocks were subject to less apparent folding and rock deformation than the Huanggangliang Formation. Tectonic stress was mainly accommodated by vertically tilting of the turbiditic layers. The Solonker Suture Zone comprises the Erdaojing and Ondor Sum Subduction-Accretion Complexes (see also Figure 2). Such collision resulting from double-sided subduction would not lead to continental deep subduction and subsequent exhumation/uplift. This type of "soft collision" [e.g., *Kröner et al.*, 2014] is consistent with the absence of high-grade metamorphic rocks and complex multiple deformation in the Xar Moron River region. It may also explain why broad suture zones, sometimes referred to as "cryptic" sutures, e.g., by *Xiao et al.* [2013] in the Chinese Tianshan, and not sharp suture lines are formed.

Acknowledgments

We appreciate the very constructive comments of editors Todd Ehlers and John Geissman, associate editor Paul Kapp, and journal reviewers Simon A. Wilde and Shoufa Lin, which led to significant improvements on the initial version of the manuscript. We would also like to thank Jason Ali for comments on late stages of the draft. This study was financially supported by a NSFC Project (41190075) entitled "Final Closure of the Paleo-Asian Ocean and Reconstruction of East Asian Blocks in Pangea," which is the fifth research project of NSFC Major Program (41190070) "Reconstruction of East Asian Blocks in Pangea," a Hong Kong RGC GRF (7063/13P), and NSFC General Projects (41230207 and 41390441). This paper is a contribution to IGCP#592.

References

Andersen, T. (2005), Detrital zircons as tracers of sedimentary provenance: Limiting conditions from statistics and numerical simulation, *Chem. Geol.*, *216*(3–4), 249–270, doi:10.1016/J.Chemgeo.2004.11.013.

Bhatia, M. R. (1983), Plate tectonics and geochemical composition of sandstones, *J. Geol.*, *91*(6), 611–627.

Bureau of Geology and Mineral Resources of Inner Mongolia (BGMRIM), Regional Geology of Nei Mongol (Inner Mongolia) Autonomous Region (1991) [in Chinese with English summary], *Geol. Mem*, Ser. 2., vol. 25, 725 pp., Geol. Publ. House, Beijing.

Cao, C. (1989), The ophiolite belts of northeastern China, *J. Southeast Asian Earth Sci.*, *3*(1–4), 233–236, doi:10.1016/0743-9547(89)90027-5.

Cawood, P. A., A. Kröner, W. J. Collins, T. M. Kusky, W. D. Mooney, and B. F. Windley (2009), Accretionary orogens through Earth history, *Geol. Soc. London Spec. Publ.*, *318*(1), 1–36, doi:10.1144/SP318.1.

Cawood, P. A., C. J. Hawkesworth, and B. Dhuime (2012), Detrital zircon record and setting, *Geology*, *40*(10), 875–878, doi:10.1130/G32945.1.

Chen, B., B. M. Jahn, S. Wilde, and B. Xu (2000), Two contrasting Paleozoic magmatic belts in northern Inner Mongolia, China: Petrogenesis and tectonic implications, *Tectonophysics*, *328*(1–2), 157–182.

Chen, B., B. M. Jahn, and W. Tian (2009a), Evolution of the Solonker suture zone: Constraints from zircon U-Pb ages, Hf isotopic ratios and whole-rock Nd-Sr isotope compositions of subduction- and collision-related magmas and forearc sediments, *J. Asian Earth Sci.*, *34*(3), 245–257, doi:10.1016/j.jseaes.2008.05.007.

Chen, B., X. H. Ma, A. K. Liu, and Z. Muhetaer (2009b), Zircon U-Pb ages of the Xilinhot metamorphic complex and blueschist, and implications for tectonic evolution of the Solonker suture, *Acta Petrol. Sin.*, *25*(12), 3123–3129.

Cogne, J. P., V. A. Kravchinsky, N. Halim, and F. Hankard (2005), Late Jurassic–Early Cretaceous closure of the Mongol-Okhotsk Ocean demonstrated by new Mesozoic palaeomagnetic results from the Trans-Baikal area (SE Siberia), *Geophys. J. Int.*, *163*(2), 813–832, doi:10.1111/J.1365-246x.2005.02782.X.

Collins, W. J., E. A. Belousova, A. I. S. Kemp, and J. B. Murphy (2011), Two contrasting Phanerozoic orogenic systems revealed by hafnium isotope data, *Nat. Geosci.*, *4*(5), 333–337, doi:10.1038/Ngeo1127.

Cope, T., B. D. Ritts, B. J. Darby, A. Fildani, and S. A. Graham (2005), Late Paleozoic sedimentation on the northern margin of the North China block: Implications for regional tectonics and climate change, *Int. Geol. Rev.*, *47*(3), 270–296.

Darby, B. J., and G. Gehrels (2006), Detrital zircon reference for the North China block, *J. Asian Earth Sci.*, *26*(6), 637–648, doi:10.1016/J.Jseaes.2004.12.005.

De Jong, K., W. J. Xiao, B. F. Windley, H. Masago, and C. H. Lo (2006), Ordovician Ar-40/Ar-39 phengite ages from the blueschist-facies Ondor Sum subduction-accretion complex (Inner Mongolia) and implications for the Early Paleozoic history of continental blocks in China and adjacent areas, *Am. J. Sci.*, *306*(10), 799–845, doi:10.2475/10.2006.02.

Dickinson, W. R. (1985), Interpreting provenance relations from detrital modes of sandstones, *Provenance Arenites*, *148*, 333–361.

Dodson, M. H., W. Compston, I. S. Williams, and J. F. Wilson (1988), A search for ancient detrital zircons in Zimbabwean sediments, *J. Geol. Soc.*, *145*, 977–983.

Gehrels, G. E., R. Blakey, K. E. Karlstrom, J. M. Timmons, B. Dickinson, and M. Pecha (2011), Detrital zircon U-Pb geochronology of Paleozoic strata in the Grand Canyon, Arizona, *Lithosphere*, *3*(3), 183–200, doi:10.1130/L121.1.

Ge, R., W. Zhu, H. Wu, and B. Zheng (2013), Zircon U-Pb ages and Lu-Hf isotopes of Paleoproterozoic metasedimentary rocks in the Korla Complex, NW China: Implications for metamorphic zircon formation and geological evolution of the Tarim Craton, *Precambrian Res.*, *231*, 1–18, doi:10.1016/j.precamres.2013.03.003.

Hall, R. (2009), Southeast Asia's changing palaeogeography, *Blumea*, *54*(1–3), 148–161, doi:10.3767/000651909x475941.

Han, G. Q., Y. J. Liu, F. Neubauer, W. Jin, J. Genser, S. M. Ren, W. Li, Q. B. Wen, Y. L. Zhao, and C. Y. Liang (2012), LA-ICP-MS U-Pb dating and Hf isotopic compositions of detrital zircons from the Permian sandstones in Da Xing'an Mountains, NE China: New evidence for the eastern extension of the Erenhot-Hegenshan suture zone, *J. Asian Earth Sci.*, *49*, 249–271, doi:10.1016/J.Jseaes.2011.11.011.

Haughton, P. D. W., S. P. Todd, and A. C. Morton (1991), Sedimentary provenance studies, *Geol. Soc. London Spec. Publ.*, *57*(1), 1–11, doi:10.1144/GSL.SP.1991.057.01.01.

Hu, Z. C., Y. S. Liu, L. Chen, L. A. Zhou, M. Li, K. Q. Zong, L. Y. Zhu, and S. Gao (2011), Contrasting matrix induced elemental fractionation in NIST SRM and rock glasses during laser ablation ICP-MS analysis at high spatial resolution, *J. Anal. At. Spectrom.*, *26*(2), 425–430, doi:10.1039/C0ja00145g.

Jackson, S. E., N. J. Pearson, W. L. Griffin, and E. A. Belousova (2004), The application of laser ablation-inductively coupled plasma-mass spectrometry to in situ U-Pb zircon geochronology, *Chem. Geol.*, *211*, 47–69, doi:10.1016/j.chemgeo.2004.06.017.

Jian, P., et al. (2008), Time scale of an early to middle Paleozoic orogenic cycle of the long-lived Central Asian Orogenic Belt, Inner Mongolia of China: Implications for continental growth, *Lithos*, *101*(3–4), 233–259, doi:10.1016/J.Lithos.2007.07.005.

Jian, P., D. Y. Liu, A. Kroner, B. F. Windley, Y. R. Shi, W. Zhang, F. Q. Zhang, L. C. Miao, L. Q. Zhang, and D. Tomurhuu (2010), Evolution of a Permian intraoceanic arc-trench system in the Solonker suture zone, Central Asian Orogenic Belt, China and Mongolia, *Lithos*, *118*(1–2), 169–190, doi:10.1016/J.Lithos.2010.04.014.

Kröner, A., et al. (2014), Reassessment of continental growth during the accretionary history of the Central Asian Orogenic Belt, *Gondwana Res.*, *25*(1), 103–125, doi:10.1016/j.gr.2012.12.023.

Lehmann, J., K. Schulmann, O. Lexa, M. Corsini, A. Kroner, P. Stipska, D. Tomurhuu, and D. Otgonbator (2010), Structural constraints on the evolution of the Central Asian Orogenic Belt in SW Mongolia, *Am. J. Sci.*, *310*(7), 575–628, doi:10.2475/07.2010.02.

Li, D. P., Y. L. Chen, Z. Wang, K. J. Hou, and C. Z. Liu (2011), Detrital zircon U-Pb ages, Hf isotopes and tectonic implications for Palaeozoic sedimentary rocks from the Xing-Meng Orogenic Belt, Middle-East Part of Inner Mongolia, China, *Geol. J.*, *46*(1), 63–81, doi:10.1002/Gj.1257.

Li, J. Y. (2006), Permian geodynamic setting of Northeast China and adjacent regions: Closure of the Paleo-Asian Ocean and subduction of the Paleo-Pacific Plate, *J. Asian Earth Sci.*, *26*(3–4), 207–224, doi:10.1016/J.Jseaes.2005.09.001.

Li, J. Y., L. M. Gao, G. H. Sun, Y. P. Li, and Y. B. Wang (2007), Shuangjingzi middle Triassic syn-collisional crust-derived granite in the east Inner Mongolia and its constraint on the timing of collision between Siberian and Sino-Korean paleo-plates, *Acta Petrol. Sin.*, *23*(3), 565–582.

Li, X. H., Z. X. Li, M. T. D. Wingate, S. L. Chung, Y. Liu, G. C. Lin, and W. X. Li (2006), Geochemistry of the 755 Ma Mundine Well dyke swarm, northwestern Australia: Part of a Neoproterozoic mantle superplume beneath Rodinia?, *Precambrian Res.*, *146*, 1–15.

Li, Y. L., H. W. Zhou, F. M. Brouwer, J. R. Wijbrans, Z. Q. Zhong, and H. F. Liu (2011a), Tectonic significance of the Xilin Gol Complex, Inner Mongolia, China: Petrological, geochemical and U-Pb zircon age constraints, *J. Asian Earth Sci.*, *42*(5), 1018–1029, doi:10.1016/J.Jseaes.2010.09.009.

Li, Y. L., H. W. Zhou, F. M. Brouwer, W. J. Xiao, Z. Q. Zhong, and J. R. Wijbrans (2011b), Late Carboniferous–Middle Permian arc/forearc-related basin in Central Asian Orogenic Belt: Insights from the petrology and geochemistry of the Shuangjing Schist in Inner Mongolia, China, *Isl. Arc*, *20*(4), 535–549, doi:10.1111/J.1440-1738.2011.00784.X.

Li, Y. L., H. Zhou, F. M. Brouwer, W. Xiao, J. R. Wijbrans, J. Zhao, Z. Zhong, and H. Liu (2013), Nature and timing of the Solonker suture of the Central Asian Orogenic Belt: Insights from geochronology and geochemistry of basic intrusions in the Xilin Gol Complex, Inner Mongolia, China, *Int. J. Earth Sci.*, *103*, 1–20, doi:10.1007/s00531-013-0931-3.

Lin, W., M. Faure, S. Nomade, Q. H. Shang, and P. R. Renne (2008), Permian-Triassic amalgamation of Asia: Insights from Northeast China sutures and their place in the final collision of North China and Siberia, *C. R. Geosci.*, *340*(2–3), 190–201, doi:10.1016/J.Crte.2007.10.008.

Liu, Y. S., S. Gao, Z. C. Hu, C. G. Gao, K. Q. Zong, and D. B. Wang (2010a), Continental and oceanic crust recycling-induced melt-peridotite interactions in the Trans-North China Orogen: U-Pb dating, Hf isotopes and trace elements in zircons from mantle xenoliths, *J. Petrol.*, *51*(1–2), 537–571, doi:10.1093/Petrology/Egp082.

Liu, Y. S., Z. C. Hu, K. Q. Zong, C. G. Gao, S. Gao, J. A. Xu, and H. H. Chen (2010b), Reappraisement and refinement of zircon U-Pb isotope and trace element analyses by LA-ICP-MS, *Chin. Sci. Bull.*, *55*(15), 1535–1546, doi:10.1007/S11434-010-3052-4.

Ludwig, K. R. (2008), Manual for Isoplot 3.7, Special Publication 4, Berkeley Geochronology Center.

Manankov, I. N., G. R. Shi, and S. Z. Shen (2006), An overview of Permian marine stratigraphy and biostratigraphy of Mongolia, *J. Asian Earth Sci.*, *26*(3–4), 294–303, doi:10.1016/J.Jseaes.2005.11.008.

Meng, F. X., S. Gao, H. L. Yuan, and H. J. Gong (2010), Permian-Triassic (260–220 Ma) crustal growth of Eastern Central Asian Orogenic Belt as revealed by detrital zircon studies, *Am. J. Sci.*, *310*(5), 364–404, doi:10.2475/05.2010.02.

Miao, L. C., W. M. Fan, D. Y. Liu, F. Q. Zhang, Y. R. Shi, and F. Guo (2008), Geochronology and geochemistry of the Hegenshan ophiolitic complex: Implications for late-stage tectonic evolution of the Inner Mongolia-Daxinganling Orogenic Belt, China, *J. Asian Earth Sci.*, *32*(5–6), 348–370, doi:10.1016/J.Jseaes.2007.11.005.

Nozaka, T., and Y. Liu (2002), Petrology of the Hegenshan ophiolite and its implication for the tectonic evolution of northern China, *Earth Planet. Sci. Lett.*, *202*(1), 89–104.

Pelto, C. R. (1954), Mapping of multicomponent systems, *J. Geol.*, *62*(5), 501–511.

Popov, V., A. Khramov, and V. Bachtadse (2005), Palaeomagnetism, magnetic stratigraphy, and petromagnetism of the Upper Vendian sedimentary rocks in the sections of the Zolotitsa River and in the Verkhotina Hole, Winter Coast of the White Sea, Russia, *Russ. J. Earth Sci.*, *7*(2), 1–29.

Rojas-Agramonte, Y., A. Kröner, A. Demoux, X. Xia, W. Wang, T. Donskaya, D. Liu, and M. Sun (2011), Detrital and xenocrystic zircon ages from Neoproterozoic to Palaeozoic arc terranes of Mongolia: Significance for the origin of crustal fragments in the Central Asian Orogenic Belt, *Gondwana Res.*, *19*(3), 751–763, doi:10.1016/J.Gr.2010.10.004.

Roser, B. P., and R. J. Korsch (1988), Provenance signatures of sandstone-mudstone suites determined using discriminant function analysis of major-element data, *Chem. Geol.*, *67*(1), 119–139, doi:10.1016/0009-2541(88)90010-1.
Şengör, A. M. C., B. A. Natal'in, and V. S. Burtman (1993), Evolution of the Altaid tectonic collage and Paleozoic crustal growth in Eurasia, *Nature*, *364*(6435), 299–307.
Shannon, C. E., and W. Weaver (1963), *The Mathematical Theory of Communication*, Univ. of Illinois Press, Urbana and Chicago.
Shao, J. (1989), Continental crust accretion and tectono-magmatic activity at the northern margin of the Sino-Korean plate, *J. Southeast Asian Earth Sci.*, *3*(1–4), 57–62, doi:10.1016/0743-9547(89)90009-3.
Shen, S. Z., H. Zhang, Q. H. Shang, and W. Z. Li (2006), Permian stratigraphy and correlation of Northeast China: A review, *J. Asian Earth Sci.*, *26*(3–4), 304–326, doi:10.1016/J.Jseases.2005.07.007.
Shi, G., M. Faure, B. Xu, P. Zhao, and Y. Chen (2013), Structural and kinematic analysis of the Early Paleozoic Ondor Sum-Hongqi mélange belt, eastern part of the Altaids (CAOB) in Inner Mongolia, China, *J. Asian Earth Sci.*, *66*, 123–139, doi:10.1016/j.jseaes.2012.12.034.
Shi, G. H., D. Y. Liu, F. Q. Zhang, P. Jian, L. C. Miao, Y. R. Shi, and H. Tao (2003), SHRIMP U-Pb zircon geochronology and its implications on the Xilin Gol Complex, Inner Mongolia, China, *Chin. Sci. Bull.*, *48*(24), 2742–2748, doi:10.1360/033wd0191.
Shi, G. R. (2006), The marine Permian of East and Northeast Asia: An overview of biostratigraphy, palaeobiogeography and palaeogeographical implications, *J. Asian Earth Sci.*, *26*(3–4), 175–206, doi:10.1016/J.Jseaes.2005.11.004.
Shi, G. R., M. J. Campi, and S. Z. Shen (2006), The Permian of East and Northeast Asia, *J. Asian Earth Sci.*, *26*(3–4), 173–174, doi:10.1016/j.jseses.2005.12.001.
Sircombe, K. N. (2004), AGEDISPLAY: An EXCEL workbook to evaluate and display univariate geochronological data using binned frequency histograms and probability density distributions, *Comput. Geosci.*, *30*(1), 21–31, doi:10.1016/J.Cageo.2003.09.006.
Sláma, J., et al. (2008), Plešovice zircon—A new natural reference material for U-Pb and Hf isotopic microanalysis, *Chem. Geol.*, *249*, 1–35, doi:10.1016/j.chemgeo.2007.11.005.
Smethurst, M. A., A. N. Khramov, and T. H. Torsvik (1998), The Neoproterozoic and Palaeozoic palaeomagnetic data for the Siberian Platform: From Rodinia to Pangea, *Earth Sci. Rev.*, *43*(1–2), 1–24.
Smosna, R., K. R. Bruner, and A. Burns (1999), Numerical analysis of sandstone composition, provenance, and paleogeography, *J. Sediment. Res.*, *69*(5), 1063–1070.
Tang, K. D. (1990), Tectonic development of Paleozoic foldbelts at the north margin of the Sino-Korean craton, *Tectonics*, *9*(2), 249–260.
Vermeesch, P. (2004), How many grains are needed for a provenance study?, *Earth Planet. Sci. Lett.*, *224*(3–4), 441–451, doi:10.1016/J.Cpsl.2004.05.037.
Wiedenbeck, M., P. Allé, F. Corfu, W. L. Griffin, M. Meier, F. Oberli, A. von Quadt, J. C. Roddick, and W. Spiegel (1995), Three natural zircon standards for U-Th-Pb, Lu-Hf, trace element and REE analyses, *Geostand. Newsl.*, *19*(1), 1–23, doi:10.1111/j.1751-908X.1995.tb00147.x.
Wilhem, C., B. F. Windley, and G. M. Stampfli (2012), The Altaids of Central Asia: A tectonic and evolutionary innovative review, *Earth Sci. Rev.*, *113*, 303–341.
Windley, B. F., D. Alexeiev, W. J. Xiao, A. Kroner, and G. Badarch (2007), Tectonic models for accretion of the Central Asian Orogenic Belt, *J. Geol. Soc.*, *164*, 31–47.
Wu, F. Y., D. Y. Sun, H. M. Li, B. M. Jahn, and S. Wilde (2002), A-type granites in northeastern China: Age and geochemical constraints on their petrogenesis, *Chem. Geol.*, *187*(1–2), 143–173.
Wu, F. Y., G. C. Zhao, D. Y. Sun, S. A. Wilde, and J. H. Yang (2007), The Hulan Group: Its role in the evolution of the Central Asian Orogenic Belt of NE China, *J. Asian Earth Sci.*, *30*(3–4), 542–556, doi:10.1016/j.jseaes.2007.01.003.
Xiao, W. J., B. F. Windley, J. Hao, and M. G. Zhai (2003), Accretion leading to collision and the Permian Solonker suture, Inner Mongolia, China: Termination of the central Asian orogenic belt, *Tectonics*, *22*(6), 1069, doi:10.1029/2002TC001484.
Xiao, W. J., B. F. Windley, B. C. Huang, C. M. Han, C. Yuan, H. L. Chen, M. Sun, S. Sun, and J. L. Li (2009), End-Permian to mid-Triassic termination of the accretionary processes of the southern Altaids: Implications for the geodynamic evolution, Phanerozoic continental growth, and metallogeny of Central Asia, *Int. J. Earth Sci.*, *98*(6), 1189–1217, doi:10.1007/S00531-008-0407-Z.
Xiao, W. J., B. C. Huang, C. M. Han, S. Sun, and J. L. Li (2010), A review of the western part of the Altaids: A key to understanding the architecture of accretionary orogens, *Gondwana Res.*, *18*(2–3), 253–273, doi:10.1016/j.gr.2010.01.007.
Xiao, W. J., B. F. Windley, M. B. Allen, and C. M. Han (2013), Paleozoic multiple accretionary and collisional tectonics of the Chinese Tianshan orogenic collage, *Gondwana Res.*, *23*(4), 1316–1341, doi:10.1016/j.gr.2012.01.012.
Xu, B., and B. Chen (1997), Framework and evolution of the middle Paleozoic orogenic belt between Siberian and North China plates in northern Inner Mongolia, *Sci. China Earth Sci.*, *40*(5), 463–469, doi:10.1007/Bf02877610.
Xu, B., J. Charvet, Y. Chen, P. Zhao, and G. Shi (2013), Middle Paleozoic convergent orogenic belts in western Inner Mongolia (China): Framework, kinematics, geochronology and implications for tectonic evolution of the Central Asian Orogenic Belt, *Gondwana Res.*, *23*, 1342–1364.
Yakubchuk, A. (2008), Re-deciphering the tectonic jigsaw puzzle of northern Eurasia, *J. Asian Earth Sci.*, *32*(2–4), 82–101, doi:10.1016/J.Jseaes.2007.10.009.
Yan, Z., T. Kedong, B. Jingwen, and M. Youchen (1989), High pressure metamorphic rocks and their tectonic environment in northeastern China, *J. Southeast Asian Earth Sci.*, *3*(1–4), 303–313, doi:10.1016/0743-9547(89)90035-4.
Zhang, S. H., Y. Zhao, B. Song, Z. Y. Yang, J. M. Hu, and H. Wu (2007), Carboniferous granitic plutons from the northern margin of the North China block: Implications for a late Palaeozoic active continental margin, *J. Geol. Soc.*, *164*, 451–463.
Zhang, S. H., Y. Zhao, A. Kroner, X. M. Liu, L. W. Xie, and F. K. Chen (2009), Early Permian plutons from the northern North China Block: Constraints on continental arc evolution and convergent margin magmatism related to the Central Asian Orogenic Belt, *Int. J. Earth Sci.*, *98*(6), 1441–1467, doi:10.1007/S00531-008-0368-2.
Zhang, X. H., H. F. Zhang, Y. J. Tang, S. A. Wilde, and Z. C. Hu (2008), Geochemistry of Permian bimodal volcanic rocks from central inner Mongolia, North China: Implication for tectonic setting and Phanerozoic continental growth in Central Asian Orogenic Belt, *Chem. Geol.*, *249*(3–4), 262–281, doi:10.1016/J.Chemgeo.2008.01.005.
Zhang, X. H., S. Wilde, H. F. Zhang, Y. J. Tang, and M. G. Zhai (2009), Geochemistry of hornblende gabbros from Sonidzuoqi, Inner Mongolia, North China: Implications for magmatism during the final stage of suprasubduction-zone ophiolite formation, *Int. Geol. Rev.*, *51*(4), 345–373, doi:10.1080/00206810802712103.
Zhou, J. B., S. A. Wilde, X. Z. Zhang, F. L. Liu, and J. H. Liu (2012), Detrital zircons from phanerozoic rocks of the Songliao Block, NE China: Evidence and tectonic implications, *J. Asian Earth Sci.*, *47*, 21–34, doi:10.1016/J.Jseaes.2011.05.004.